Article

Bacterial Motility Reveals Unknown Molecular Organization

Ismaël Duchesne,[1] Simon Rainville,[1,*] and Tigran Galstian[1]
[1]Department of Physics, Engineering Physics and Optics and Center for Optics, Photonics and Lasers, Laval University, Quebec City, Quebec, Canada

ABSTRACT The water solubility of lyotropic liquid crystals (LCs) makes them very attractive to study the behavior of biological microorganisms in an environment where local symmetry is broken (as often encountered in nature). Several recent studies have shown a dramatic change in the behavior of flagellated bacteria when swimming in solutions of the lyotropic LC disodium cromoglycate (DSCG). In this study, the movements of *Escherichia coli* bacteria in DSCG-water solutions of different concentrations are observed to improve our understanding of this phenomenon. In addition, the viscosity of DSCG aqueous solutions is measured as a function of concentration at room temperature. We also experimentally identify a previously undescribed isotropic pretransition zone where bacteria start sticking to each other and to surfaces. Simple estimations show that the unbalanced osmotic pressure induced depletion force might be responsible for this sticking phenomenon. An estimate of the bacteria propulsive force and the DSCG aggregates length (versus concentration) are calculated from the measured viscosity of the medium. All these quantities are found to undergo a strong increase in the pretransition zone, starting at a threshold concentration of 6 $\pm$ 1 wt % DSCG that is well below the known isotropic-LC transition (~10 wt %). This study also shines light on the motility of flagellated bacteria in realistic environments, and it opens new avenues for interesting applications such as the use of motile microorganisms to probe the physical properties of their host or smart bandages that could guide bacteria out of wounds.

INTRODUCTION

Many biological processes occur under a very delicate balance of forces. Weak disturbances in this equilibrium may bring drastic changes to these processes. For instance, the swimming of flagellated bacteria is subject to multiple forces and constraints, and it was recently shown that this behavior dramatically changes in anisotropic environments (whose properties vary with direction) (1–5). Interestingly, many natural environments show some level of anisotropy. For example, several studies have shown that a liquid crystal (LC) phase (anisotropic phase) can be observed in a solution of isolated biological molecules such as chitin or collagen (6). Even if the concentration needed to obtain this anisotropic phase is generally higher than those found in nature, we expect that environments enriched with those molecules can have local LC domains. Natural mucus can also show an LC phase when it is exposed to air for a few hours (7–9). This state could be necessary to form the compact granule of mucus found in mucosa cells (7). Synovial fluid, used for the lubrication in cartilage, is also known to be an LC (10). Some motile bacteria can be found in this lubricant, for instance *Borrelia burgdorferi*, which is responsible for the Lyme disease, *Pseudomonas aeruginosa*, and *Yersinia enterocolitica* (11,12). Finally, although biofilms are not strictly speaking LCs, they can exhibit anisotropic properties (13,14), and a recent study has shown that swimming bacteria can infiltrate the biofilm, enhancing its viability or in some cases, causing its destruction (15).

Although the use of LCs in consumer electronic products (such as displays (16) and lenses (17)) has been widely explored in the scientific literature, their combination with biological systems, for diagnostics (18) and sensing (19), is relatively recent. Because they are biocompatible, aqueous solutions of lyotropic LCs have been used in several recent reports to study the behavior of flagellated bacteria in anisotropic environments. Exciting research was conducted in many groups to extend these studies to the behavior of several types of bacteria in biocompatible LCs. The three-dimensional (3D) random trajectories followed by bacteria swimming in an aqueous (isotropic) environment (20–22) have been shown to be radically modified by the presence of an orientational order in the motility medium (2–5). For example, it was shown that individual bacteria move along (forward and backward) the direction of the anisotropy axis in a lyotropic LC environment (water solution of disodium cromoglycate, DSCG) (2). It was also discovered that the presence of bacteria in such medium may result in a delicate coupling of the orientational order and bacterial activities resulting in local phase transitions (3). Finally, an orientational deformation mediated sticking (or trapping) between two bacteria has been observed in the anisotropic phase of the host (15 wt % DSCG) (4), and the interface between coexisting isotropic and LC phases has been used to probe how mechanical anisotropy and defects in LC ordering influence fundamental bacterial behaviors (5).

Submitted March 25, 2015, and accepted for publication September 21, 2015.

*Correspondence: simon.rainville@phy.ulaval.ca

Editor: Dennis Bray.

0006-3495/15/11/2137/11

http://dx.doi.org/10.1016/j.bpj.2015.09.033

In this work, we present a detailed study of the bacterial motility at different concentrations of DSCG, bringing the medium from isotropic to anisotropic states. Our results uncover a previously undescribed (to the best of our knowledge) pretransition zone between the isotropic and anisotropic phases. Measurements of the viscosity of the solution as a function of DSCG concentration show an exponential increase in viscosity in this pretransition zone (after a threshold of ~6 wt % DSCG that is well before the nematic transition occurring at 10 to 11 wt %) that we attempt to understand using a qualitative model of the DSCG molecules' aggregation.

MATERIALS AND METHODS

Cell culture

Escherichia coli (*E. coli*) strain HCB33 (wild-type, the same strain as RP437 (23)) was used in our experiments with motile bacteria and strain JY25 (wild-type modified to obtain a strain without filament, Δ*cheY* and Δ*fliC* in HCB33 (24)) in those with nonmotile bacteria. Single bacterial colonies were grown on agar plate (15 g agar, 10 g Bacto-Tryptone, and 5 g NaCl in 1 liter) at 37°C for 24 h. Then, bacteria from one colony were picked and grown to saturated phase in Terrific Broth (10g Bacto-Tryptone and 5g NaCl in 1 liter) at 34°C for 15 h in a shaking incubator at 200 rpm. Next, 100 μl of saturated culture was diluted in 10 ml of Terrific Broth and grown to exponential phase at 34°C for 4 h in a shaking incubator at 200 rpm. The cells were washed once with motility buffer (MB) (10 mM KPO_4, 0.1 mM EDTA, 10 mM lactic acid, and 20 mM glucose) and then suspended in ~5 ml of MB to obtain a bacterial concentration of OD_{600} ~ 0.8. Finally, 20 μl from this suspension was diluted into a DSCG solution at the desired concentration to obtain a total volume of 160 μl.

LC mixture

The DSCG (Sigma-Aldrich, St. Louis, MO) was used to prepare the solution of LC. To make different concentrations of DSCG LC, a stock solution was made by mixing 16.0 wt % DSCG with 84 wt % MB. This mixture was heated for at least 10 min at 55°C and then shaken for ~1 min to ensure complete solubility. The stock solution was stored at 4°C. Before making the final DSCG solution, the stock solution was heated again for 5 min at 55°C and shaken for 1 min to ensure complete homogeneity. A small amount of the stock LC was then diluted into a solution with a total volume of 160 μl containing a concentration of either bacteria of OD_{600} ~ 0.15 or polystyrene microspheres (see below) with a diameter of 0.75 μm (Polysciences, Warrington, PA) to obtain a DSCG concentration from 0 to 13.7 wt %. The temperature in all our experiments was 22.5°C ± 0.5°C. At this temperature, DSCG forms a nematic LC phase above ~11 wt % and an isotropic phase below ~10 wt %. Between these two concentrations both phases coexist. The detailed concentration/temperature phase diagram of the mixture may be found in Lydon (25).

LC chamber

To make an optical chamber for our experiment, a coating of PI-150 1% (Nissan Chemical, Houston, TX) was first applied onto two glass cover slips by spin coating. This surface was then rubbed unidirectionally with a technique described in Seo et al. (26). Finally, a cavity was created by sticking together two cover slips with UV glue (Optical Adhesive 65, Norland, Cranbury, NJ) containing 60 μm glass microspheres used as spacers (Duke Scientific, Palo Alto, CA) (see Fig. S10 in the Supporting Material for more information and Duchesne et al. (27)). The solution was inserted by capillarity in the sandwich-like chamber. To prevent the movement of fluid and evaporation of water, the chamber was closed with transparent nail polish. Results obtained for each concentration were measured with at least three different samples made from at least two different stock solutions.

Bacteria observations

To visualize bacteria and microspheres, an IX71 Olympus inverted microscope equipped with crossed polarizers and an EMCCD iXon3 888 camera (Andor Technology, South Windsor, CT) was used. To observe the motility of bacteria, a 60× oil objective with 1.25NA (Olympus UPLFLN 60XOIPH, Tokyo, Japan) was employed in brightfield microscopy. Videos between 5 and 10 s long at a frame rate of 30 fps were recorded using a custom LabVIEW program (National Instruments, Austin, TX).

Videos of motile bacteria were analyzed with a custom particle tracking algorithm in MATLAB (The MathWorks, Natick, MA). To determine the average speed of bacteria for each concentration of DSCG, the centroids of every bacterium in each frame were identified and then linked together to create a trajectory. The difference in the bacterium position between two consecutive frames was divided by the acquisition time of the camera to obtain the instantaneous speed. Then, the average speed for every trajectory at the same concentration was computed. The image moment of every cell in each frame was used to obtain the angle between the long axis of the rod-shaped bacterium and the horizontal axis. Finally, the standard deviation of this angle for every trajectory at the same concentration was computed. Trajectories with less than 20 frames were discarded.

Viscosity measurements

To measure the effective viscosity along the axis parallel and perpendicular to the director **n** (showing the axis of the anisotropy of the LC (28)), the Brownian motion of polystyrene microspheres (with a diameter of 0.75 μm) was recorded by using the technique described in Duchesne et al. (27) (see also Saveyn et al. (29)). To visualize those particles, a guided-light dark-field microscope (27) with a 50× objective with 0.5 NA (Olympus LMPLFLN 50X, Tokyo, Japan) was used. For the calculation of the viscosity values sensed in each direction (1D), the following equation was used:

$$\eta = \frac{kT\Delta t}{6d\langle SL\rangle^2}, \quad (1)$$

where k is the Boltzmann constant, T is the temperature in Kelvin, Δt is the acquisition time, d is the diameter of the microspheres, and $\langle SL\rangle$ is the average step length executed in Δt. The weighted average viscosity for every DSCG concentration was computed from these data. The orientation of **n** was determined by using the technique described in Duchesne et al. (27). The mean squared displacement (MSD) was plotted as a function of time to make sure that the diffusion of microspheres was always normal, i.e., that the relationship was linear (27,30,31). Trajectories with less than 10 frames were discarded.

RESULTS

Motility of bacteria in anisotropic environment

This work began by carefully recording the trajectories of more than 1800 *E. coli* bacteria swimming in water solutions of DSCG with concentrations varying from 0 to 13.7 wt %. Above these concentrations, the motility of the bacteria is strongly reduced and it becomes difficult to track them. Fig. 1 shows the dramatic contrast between typical

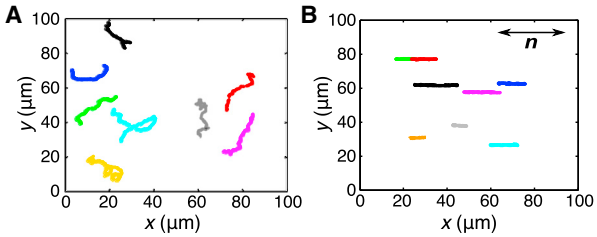

FIGURE 1 Trajectories of motile bacteria in isotropic and anisotropic solutions. (*A*) *E. coli* swimming tracks in isotropic media at 0 wt % DSCG and (*B*) in anisotropic media at 12 wt % DSCG (at 22.5 ± 0.5°C). In (*B*), the *x* axis is parallel to the rubbing direction of the chamber. To see this figure in color, go online.

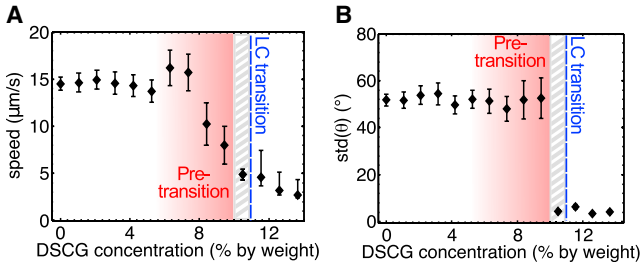

FIGURE 2 Characterization of the motility of bacteria in DSCG solutions. (*A*) Bacterial speed and (*B*) standard deviation of the orientation of the bacterial body as a function of the DSCG concentration. The standard deviation (SD) was used as the error bars. All experiments were made at 22.5 ± 0.5°C. The number of data acquired for each concentration is shown in Table S3 (1808 individual bacteria in total, and more than 83,500 positions). The gray hatched zone represents the DSCG concentration range where both phases coexist (isotropic and anisotropic). The gradient shaded zone represents the DSCG concentration range where the pretransition phenomena are observed (see main text for details). To see this figure in color, go online.

trajectories (the position of the center of gravity versus time) of bacteria recorded in isotropic and anisotropic phases (at low and high DSCG concentrations, respectively). In the anisotropic (nematic) phase of the medium (Fig. 1 *B*), all bacteria swim along a single axis in both directions, that is they make forward and backward movements in one dimension (1D). This behavior is very different from the random 3D movements observed in isotropic media ((20) and Fig. 1 *A*). Because the distance between the sample and the microscope objective is fixed during the acquisition of each movie, our recorded tracks are two-dimensional projections of the 3D trajectories. That explains why the tracks are relatively short in the isotropic phase (1 s on average) because bacteria disappear from the image when they move by more than a few micrometers out of focus. In the anisotropic regime, the tracks appear even shorter, but it is only because of the lower bacterial speed and their forward and backward movements in 1D. These data confirm that, as previously reported in earlier studies (2–4), the bacterial trajectories in an anisotropic medium are confined to the direction of **n**.

Analysis of the recorded videos also lead to the measurement of the mean speed of bacteria and the variations in the bacterial body orientation as a function of DSCG concentration. Fig. 2 *A* shows, the speed in the isotropic phase (from 0 to 7 wt % DSCG) does not change significantly and has a value of ~15 μm/s as previously reported in the literature (20–22). The speed starts to decrease at 8 wt % and, after the LC transition (above ~10 wt %), the speed slows down significantly to ~5 μm/s at 10.5 wt % and continues to decrease to reach a value of ~2.5 μm/s at 13.7 wt %. Note that the speed in the biphasic region (at 10.2 wt %) has been recorded in zones where the solution exhibited a nematic phase.

To quantify the degree of unidirectionality of the bacterial trajectories, the standard deviation of the bacterial body orientation angle was computed (shown on Fig. 2 *B*). We observe that the bacteria orientations are randomly distributed in the isotropic environment (because the standard deviation of a random distribution with values between 0° to 180° is ~52°), whereas the bacteria are all aligned along one direction in the anisotropic environment (the standard deviation of the angle is ~4°).

Pretransition zone

Although some of the above-mentioned behaviors had already been reported (2), this much larger and detailed study led to the observation of an unexpected and distinct behavior of bacteria between 6 and 10 wt % DSCG concentration. In this concentration interval (further referred to as the pretransition zone), the bacteria experience significant difficulties for swimming; they are very sticky and stop swimming as soon as they touch any surface or other bacteria (see Section S5 for examples of images). In some rare cases, bacteria are able to detach themselves and swim away, but most of the time they remain stuck. When the bacterial concentration was raised to OD_{600} ~ 3, big aggregates of bacteria were formed. At a DSCG concentration below 6 wt %, this sticky behavior is rarely observed, but it becomes more common as the concentration increases, up to 10 wt %. Because of that effect, the number of swimming bacteria that could be tracked in this region is limited. It is difficult to determine if the sticky effect is still present above 10 wt % because, in the anisotropic phase, each bacterium moves along its own straight line, so that collisions with the chamber's top and bottom surfaces occur much less often and that collision between bacteria are described by the elastic interactions (4) (which is different from the interactions observed in the pretransition zone, see Discussion).

Viscosity of the DSCG solution

The swimming of *E. coli* is characterized by a low Reynolds number ($Re \sim 10^{-4}$), which means that the viscous forces are much more important than the inertial forces (32).

Obviously, the elastic forces, involved in the deformation of the aligned LC environment, also play an important role at high DSCG concentration when the medium is anisotropic (4). However, the pretransition zone described above is not in the anisotropic LC phase. To investigate what could cause the existence of three distinct regimes in bacterial motility (purely isotropic, pretransition, and anisotropic regimes), we measured the effective viscosity of the medium in the directions parallel and perpendicular to **n**. To do so, the Brownian diffusion of more than 11,800 polystyrene microspheres (with a diameter of 0.75 μm) was tracked in DSCG solutions of various concentrations (in motility buffer MB). Fig. 3, *A* and *B*, shows typical trajectories of microspheres diffusing in isotropic and anisotropic environments. As expected, the average distance traveled by microspheres in isotropic media is identical in any direction, which is not the case in anisotropic media. The viscosity was measured from these trajectories (see Duchesne et al. (27) for details), and the results can be seen in Fig. 4. The viscosity of DSCG solutions increases very slightly at low concentration, but it suddenly starts to increase exponentially ~6 wt %. Up to ~10 wt % (the LC transition), the viscosity is the same in every directions, but, not surprisingly, the viscosity in the direction parallel to the director becomes lower than the one in the perpendicular direction once the system enters its anisotropic phase (28). The ratio of viscosities in these two directions is measured to be ~2.2 $\pm$ 0.1. This ratio is rather large compared with thermotropic LCs as IS-8200, 5CB, or MBBA (ranging from 1.35 to 1.7) (30,33,34). Above 10 wt % (the LC transition), the viscosity in the two directions still increases exponentially, but at lower rate. To our knowledge, this is the first complete study of the viscosity of DSCG solutions as a function of concentration, and the first measurement of the ratio between the viscosities perpendicular and parallel to the director in the anisotropic phase.

Interestingly, the three distinct regimes observed in the viscosity measurements correspond very closely to the three different types of behaviors we have observed in the motility of bacteria. In the purely isotropic regime, at low concentration of DSCG, bacteria swim as they usually do in water and the viscosity changes very little. In the second regime, the bacteria become very sticky and the viscosity increases exponentially. In the third regime, the bacterial trajectories and the viscosity become anisotropic along with noticeable slowing down of the viscosity growth (Figs. 2 and 4). It is certainly expected that the viscosity would increase with DSCG concentration, but we are not aware of any previous report of the three regimes described above (some pretransitional fluctuations, when the temperature of the solution is changed at constant DSCG concentration, were studied in Nastishin et al. (35)).

Note that the measured viscosity is independent of the microsphere diameter (in the range of bead diameters that we explored, between 0.2 and 2 μm, the difference was at most 20%; see Duchesne et al. (27) for details), so we only used beads of 0.75 μm diameter. Furthermore, we performed the same viscosity measurements in distilled (DI) water and the results were similar (27). Finally, to complete the analysis of the diffusion data, the relation between the MSD and time was computed. For every concentration of DSCG, the relationship between the MSD and time was linear (see Section S1). The diffusion of particles in the nematic phase of DSCG solution is therefore normal on a timescale above the minimal acquisition time we used during our experiments, namely 0.4 s. This result is in agreement with a previous report that showed anomalous diffusion only below 0.5 s in 13 wt % DSCG solution (30) (see also Duchesne et al. (27)).

Finally, it is useful to know that the alignment and anchoring of the director on the surface of the polystyrene particles and of *E. coli* is tangential. As Fig. 3, *D* and *F*, shows, the light pattern around particles, taken with crossed polarizers, is typical of a tangential surface anchoring (36,37).

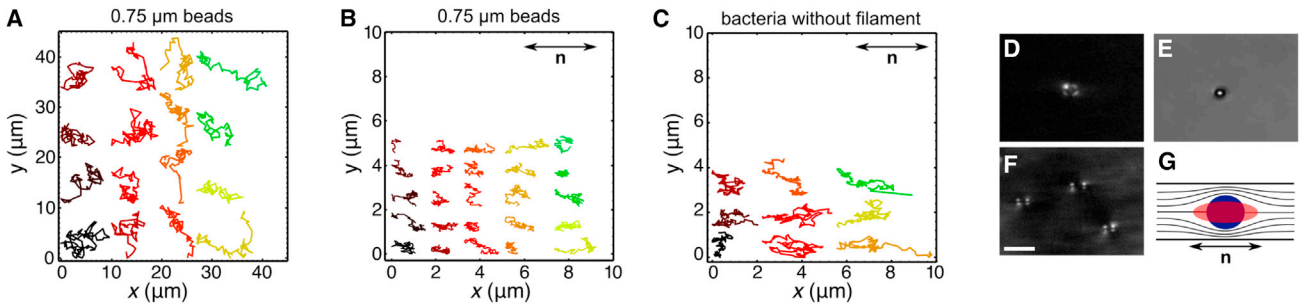

FIGURE 3 Diffusion of beads and nonmotile bacteria in DSCG solutions and anchoring of the DSCG molecules on their surfaces. (*A*) Trajectories of the diffusion of 0.75 μm diameter microspheres in an isotropic solution with 0 wt % DSCG and (*B*) in an anisotropic solution with 13.2 wt % DSCG. (*C*) Trajectories of the diffusion of paralyzed bacteria (without flagellum) in a solution with 13.2 wt % DSCG. (*D*) Image of a 3 μm polystyrene microsphere taken in brightfield with crossed polarizers and (*E*) without polarizers. (*F*) Image of three bacteria taken between crossed polarizers and (*G*) schematic representation of the perturbation of **n** around a polystyrene microsphere (*circle*) and a bacterium (*ellipse*). All experiments were made at 22.5 $\pm$ 0.5°C. The white bar in (*F*) measures 10 μm. To see this figure in color, go online.

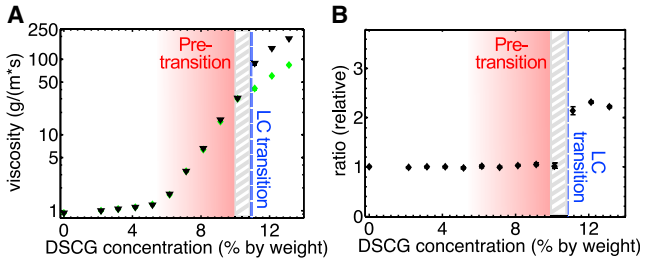

FIGURE 4 Characterization of the viscosity of DSCG solutions. (*A*) Viscosity parallel (*diamonds*) and perpendicular (*triangles*) to **n** and (*B*) anisotropy of the viscosity of DSCG solution as a function of concentration. Microspheres with a diameter of 0.75 μm were used. Each point was measured from a data set containing at least 230 microspheres and 8000 positions (11,800 individual microspheres in total, and more than 270,000 positions). The standard error of the mean was used as the error bars, but these are generally too small to be visible in figures. The unit of viscosity is equivalent to (mPa s) or cP. To see this figure in color, go online.

DISCUSSION

Propulsive force of bacteria

Many bacteria (for example, *E. coli* and *Salmonella*) swim by rotating their flagella, which are long helical filaments anchored in the membrane by a rotary motor (38). Because the physical properties of the medium change with DSCG concentration, it is relevant to ask whether the propulsive force generated by the bacterial flagella also varies. When bacteria swim, the propulsive force applied by the flagella rotation must be equal to the drag force. To estimate this propulsive force, we approximated the shape of the bacterial body by a prolate spheroid (see Fig. 5 *A*). The propulsive force we calculate is an approximation because the following two effects are ignored: 1) the drag force on the filament (to our knowledge this calculation has never been done), and 2) the viscosity dependence on the speed of the object because this relation is unknown. In the particular case where the spheroid moves along its long axis, the drag force is described by the following equation (39):

$$F = -\frac{4\pi a\eta v}{\ln\frac{2a}{b} - \frac{1}{2}}, \qquad (2)$$

where η is the viscosity, v is the speed, a is the semi-major axis, and b the semi-minor axis of the spheroid. Our speed and viscosity measurements can thus be used to calculate the propulsive force exerted by the bacteria for each DSCG concentration. We estimated $a = 1.5 \pm 0.4$ μm and $b = 0.5 \pm 0.1$ μm from the images in our videos. In the anisotropic phase, the viscosity parallel to **n** was used for the calculation. The propulsive force that we find in MB (0 wt %) is in agreement with the one obtained for *E. coli* in previous reports, namely ~0.19 pN for our bacteria strain with a swimming speed of 15 μm/s compared with 0.32 pN for bacteria strain with a swimming speed of 30 μm/s (40). Interestingly, the propulsive force increases linearly both in the pretransition zone and in the anisotropic phase, whereas it remains stable for lower DSCG concentration (Fig. 5 *B*). Two principal hypotheses could explain this increase in propulsive force: either the torque provided by the motor increases or the propulsion efficiency is higher. The flagellar motor can work in two distinct regimes: 1) at high angular speed (high swimming speed) the torque exerted by the motor increases linearly when the speed decreases, and 2) at low angular speed (low swimming speed) the torque remains constant. Calculations show that the variable torque regime could explain the increase in the propulsive force only below a DSCG concentration of 7.2 wt % (Section S2). Above that concentration, the torque should remain constant and we therefore conclude that the observed increase in propulsive force is because of a higher propulsion efficiency. A similar situation arises in unbranched polymer solutions (non-Newtonian fluid) where the bacteria are observed to swim faster when the solution viscosity is increased. This phenomenon is believed to be caused by the interaction of the flagella with the structured network created by the unbranched polymers in the solution (41–44). A recent report has demonstrated that this phenomenon could rather be explained by the fact that the filaments see a different viscosity than the body does (39). We think that the same effect is observed here in the pretransition zone: the length of the DSCG aggregates must become suddenly long enough to form a nonaligned (isotropic) structured network (non-Newtonian solution). Below the 6 wt % threshold, the aggregates are presumably much smaller, and the solution is Newtonian.

It is also instructive to compare the speed of the bacteria as a function of the viscosity of the DSCG solution (see Fig. S11) with the speed obtained in previous work in viscous solution of long polymers. We then find that the

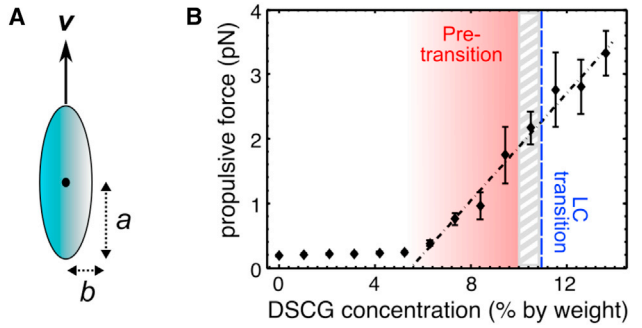

FIGURE 5 Propulsive force of the bacteria in DSCG solutions computed by modeling the shape of bacteria with a prolate spheroid. (*A*) Transversal cut of a prolate spheroid moving in the direction of its major axis and (*B*) estimation (using our viscosity measurements) of the propulsive force applied by the bacteria when it swims as a function of the DSCG concentration. The linear increase of the propulsive force (with a slope of [0.42 $\pm$ 0.09]pN/%) is represented in (*B*) with the dotted line. The gray hatched zone represents the DSCG concentration range where both phases coexist (isotropic and anisotropic). To see this figure in color, go online.

speed in the pretransition zone is similar to the speed in solution with the same viscosity, but that the speed in the anisotropic phase is higher. Indeed, in the pretransition zone, at a viscosity of 15 ± 0.2 g/(m × s), we obtain a relative speed of ~$(v_0/2)$ (where v_0 is the speed in MB) as in solutions of linear polymers (39,45). Therefore, the solutions of DSCG in the pretransition zone seem to have the same properties as the solutions of long linear polymers. In the anisotropic phase, the relative speed of the bacteria is ~$(v_0/5)$ at a viscosity of 84 ± 1 g/(m × s). This is similar to the speed measured in Martinez et al. (39), but the viscosity was ~35 g/(m × s) in that case. In addition, that speed is higher than the one obtained in Atsumi et al. (45), namely $v_0/12$ at a viscosity of ~100 g/(m × s). We therefore conclude that the anisotropic phase of DSCG solutions exhibit non-Newtonian properties that are more important than in solutions of linear polymers.

Sticky behavior

In an earlier study (25), Lydon presented a phase diagram for the DSCG-water solution (versus temperature and concentration), according to which, at room temperature, the material undergoes a phase transition starting from ~8 wt % DSCG. The zone between 8 and 12 wt % is labeled as a two-phase region. In our experiments however, this two-phase region was observed only between 10 and 11 wt %; no nematic domains were observed below 10 wt % (see Section S5) and the medium in the pretransition zone was always isotropic. Thus, the sticky behavior we observed seems to be different from the trapping by elastic forces (to minimize the elastic energy of deformation of the **n** field), described by Mushenheim et al. (4). Our observation that some bacteria succeed to break apart in the pretransition zone further supports the above statement. Indeed, for the separation to be possible, the sticky force must be of the same order of magnitude as the propulsive force produced by our bacteria, which is ~2 pN (see Fig. 5 *B* and Mushenheim et al. (4)). This force is much weaker than the trapping elastic force on similar bacteria in a solution of 15 wt % DSCG estimated in (4). Interestingly, although our force estimates show that the pretransition sticking process is weaker than the trapping elastic forces in the anistropic phase (above 10 wt % DSCG), we do not observe the same type of sticking phenomenon in the latter phase. As mentioned before, this might simply be because of the fact that interactions with surfaces are much less frequent and because the interactions between two bacteria are dominated by the elastic forces in an anisotropic medium. If the elastic deformation forces are absent in the pretransition zone, then the attraction between bacteria and surfaces must originate from other local (e.g., electrostatic or depletion) interactions.

Because the aggregates' length should increase in the pretransition zone (see section below), one could also imagine that the formation of some microscopic phase transition (that would not be observable by the techniques we are using, see also Lydon (25)) might cause the sticky effect. However, by increasing the temperature up to 37°C in a solution with 9.2 wt % DSCG, we observe no difference in the stickiness of bacteria (compared with our observations at 22.5°C). Because the local anisotropic phase should become isotropic at 37°C, this scenario becomes less plausible.

In colloidal suspension, when big particles are in the presence of much smaller ones, a depletion effect is observable. In this process, when the distance between the surfaces of two big particles become smaller or equal to the characteristic size of the small particles, the latter have the tendencies to be exclude from the space between the big particles. This exclusion create an unbalanced osmotic pressure that causes an effective force pushing together the big particles (46,47). The depletion effect becomes particularly important when the size of the small species becomes much larger than the molecular size. This phenomenon has been shown to form aggregates of bacteria in solutions with large molecules or polymers (48,49). Interestingly, this aggregation can be reversed simply by shaking the solution. Because the DSCG aggregates' length should suddenly become larger in the pretransition zone (see below), the depletion effect should also drastically increase in this zone. To verify whether the depletion force is sufficient to explain the sticky effect in the pretransition zone, we estimated the strength of this effect by considering the bacteria as big spheres and the aggregates as small rods (see Section S3) (46,47). We estimated this force by using the aggregation model of the DSCG described below for the concentrations between 6.2 and 10.2 wt %. The maximum depletion force (when the membranes of the two bacteria are in contact) increases from 90 pN at 6.2 wt % to 150 pN at 10.2 wt % (see Fig. S3). Thus, the strength of the depletion force is more than enough to create the sticky effect observed between the bacteria because the propulsive force in the pretransition zone is ~2 pN. However, we observed that some bacteria in the pretransition zone are able to detach themselves from surfaces or bacterial aggregates, suggesting that the propulsive force must be of the same order of magnitude as the sticky effect. We estimated the critical distance between two bacteria needed to have the same depletion force as the propulsion force (see Fig. S3, *inset*), and we found that it vary from ~5 nm at 6.2 wt % to ~12 nm at 9.2 wt %. We expect that the wall of two bacteria cannot be fully in contact because there are many proteins at the surface of the membrane that cause many protuberances. This should increase the minimal interbacterial distance and reduce the maximum effective depletion force sensed by the bacteria. Furthermore, the depletion effect can be perturbed by the propulsive apparatus (e.g., a filament can penetrate between the two bacteria) causing the effective force to be reduced.

We think that the depletion effect is the main mechanism that explains the sticky effect in the pretransition zone because it is in agreement with several of our observations. 1) The bacteria in aggregates can be momentarily resuspended in the solution by shaking the chamber, just like the bacterial aggregates caused by the depletion effect reported in Schwarz-Linek et al. (48). 2) Because the aggregates' length should drastically increase in the pretransition zone, the depletion force should be much more important in that zone, as the sticky effect. 3) The maximum depletion force being larger than the propulsive force, it can explain why the majority of bacteria stay stuck to each other or to the wall of the chamber. 4) Even if the propulsion force is smaller than the maximum possible depletion force, the imperfection on the surface of the bacteria and the perturbation created by the flagellar motor can explain why some bacteria are able to detach from the aggregates because the minimal distance needed for two bacteria to detach is relatively small. 5) Finally, the depletion effect can also explain why the sticky effect becomes more important as the DSCG concentration is raised because the depletion force increases with the length of the aggregates (growing with the DSCG concentration).

Aggregates length

Our measurements show that the medium's viscosity is undergoing a drastic (exponential) increase in the pretransition zone, but the link between this increasing viscosity and the stickiness of bacteria was not clear initially. Many models describe how the viscosity of a fluid increases when molecules or particles in solution aggregate (50–53). Using the Krieger and Dougherty model (53,54), we calculated how the DSCG aggregates increase in length in the pretransition zone, as the increase in propulsive force seems to suggest. This section will describe the details of this calculation.

The Krieger and Dougherty model (53,54) is one of the models that describe the behavior of the viscosity when rigid spheres form clusters in a solvent. We used this theory to estimate the length of DSCG aggregates in our system. In this model, the following equation describes the relative viscosity of the solution:

$$\eta_r = \left(1 - \frac{\phi_a}{\phi_m}\right)^{-[\eta]\phi_m}, \tag{3}$$

where $[\eta]$ is the intrinsic viscosity and ϕ_m is the volume fraction of particles in an aggregate. The volume fraction of aggregates in the solution is given by $\phi_a = \phi(r_a/r_p)^{3-d_f}$, where ϕ is the volume fraction of particles in the solution, r_a is the aggregates radius, r_p is the particles radius, and d_f is the fractal dimension of aggregates. The relative viscosity η_r is given by η/η_0, where η is the viscosity of the solution and η_0 is the viscosity of the solvent without particles.

To estimate the length of DSCG aggregates from the viscosity of the solution, we have to make some assumptions. First, we assume that aggregates are assembled from stacked disks formed by two DSCG molecules. These molecules are coupled by the aromatic rings to maximize the distance between the charged groups on the opposite side (see Fig. 6). This model is based on the conclusions of Dickinson et al. (55). The space between two disks is 0.34 nm (56), so the thickness of the disk is chosen to be also 0.34 nm (Fig. 7 *d*), which means that there is no empty space between two disks. At the DSCG concentrations considered in this work, we suppose that molecules are always coupled two by two, in agreement with an earlier study (25). Therefore single particles are considered to be disk of two DSCG molecules (with a radius r of 1 nm). Furthermore, we assume that the volume occupied by a disk in the solution does not change when they are in aggregates. The measured volume fraction ϕ at each weight fraction is shown in Table S1.

Another assumption is that the shape of the aggregates is estimated to be spheroid to simplify the calculation of $[\eta]$ (see Fig. 7). In that case, the expression for $[\eta]$ is given by the following (57):

$$[\eta] = \nu \frac{N_a}{M} v_h, \tag{4}$$

where N_a is the Avogadro constant, M is the molecular weight of aggregates, and v_h is the hydrodynamic volume of aggregates. For an oblate spheroid (disk-like), ν is given by the following:

$$\nu = \frac{16 J_o}{15 \arctan J_o}, \tag{5}$$

where $J_o = 2r/L$ (57). For a prolate spheroid (rod-like), ν is given by the following:

$$\nu = \frac{J_p^2}{15 \ln(2J_p) - \frac{3}{2}}, \tag{6}$$

where $J_p = L/2r$.

To obtain the length of the aggregates, the equivalent Stokes radius of a spheroid is used to calculate r_a. This

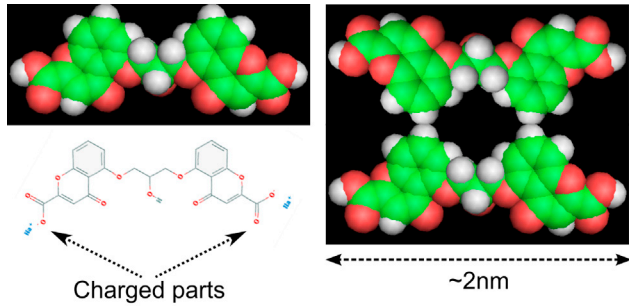

FIGURE 6 Scheme of a DSCG molecule and disk-like arrangement. To see this figure in color, go online.

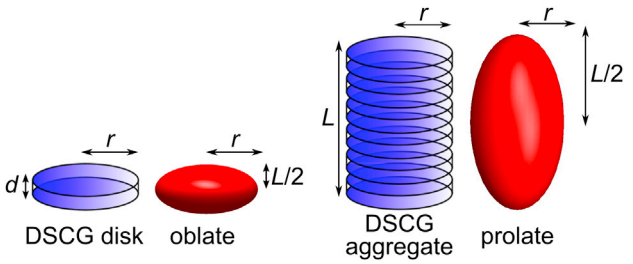

FIGURE 7 Scheme of DSCG disk and aggregate and their representation as spheroid. To see this figure in color, go online.

radius is given by the following (the Stokes radius of a spheroid corresponds to the radius of a sphere with the same volume):

$$r_s = r_a = \left(\frac{r^2 L}{2}\right)^{\left(\frac{1}{3}\right)}. \quad (7)$$

By using Eqs. 3 and 7 and isolating L, the aggregate length, on the left side of Eq. 3, we find the following:

$$L = 2\frac{r_p^3}{r^2}\left[\frac{\phi_m}{\phi}\left(1 - \eta_r^{-\left(\frac{1}{[\eta]\phi_m}\right)}\right)\right]^{\left(\frac{3}{3-d_f}\right)}. \quad (8)$$

Because $[\eta]$ depend also on L, the value of $[\eta]$ in the exponent was varied numerically to obtain the same value of L in the equation of $[\eta]$ than in Eq. 8 with a precision of 0.01 nm.

The numerical values of the different constants used in the calculation are summarized in Table S4. The volume fraction of molecules in aggregates consists in the ratio between the volume occupied by a molecule and the volume occupied by holes in an aggregate. In DSCG, this factor does not change with the size of the aggregates because of their rod-shaped symmetry. Furthermore, we suppose the arrangement of disk to be densely packed with $\phi_m = 0.9$, a value similar to the aggregation of hard spheres (50). The hydrodynamic volume of aggregates involves a comparison between the volumes occupied by DSCG molecules and by the solvent in an aggregate, multiplied by M/N_a. As for a hard sphere, we suppose that no solvent enters inside the holes of the aggregates because the center hole is exposed to the hydrophobic parts of the DSCG molecule (Fig. 6, *uncharged parts*). Therefore, $v_h = M/N_a$ and $[\eta] = \nu$. Finally, by observing the geometry of the aggregate (Fig. 7, *cylinder*), one finds that the length of the aggregate increases by one unit of length (the thickness of the DSCG disk) for each added disk, which corresponds to a fractal dimension of $d_f = 1$. Even if a more detailed model of the aggregates were to lead to a more precise value of d_f, that would simply affect the size of the aggregates, but not our conclusions.

As Fig. 8 shows, the calculated length of aggregates is stable for DSCG concentrations below 6.2 wt % for MB solutions and 7.2 wt % for DI water solutions, and it dramatically increases above this concentration. After the LC transition, the calculation indicates that length of aggregates slightly decreases, which is probably not realistic. It is important to note that this model does not take into account any electrostatic forces between aggregates, so the breakdown of the model at high concentrations is not surprising.

Additional information about motility conditions

In contrast to the results presented in Fig. 2 *A*, Kumar et al. (2) did not observe a significant difference in bacterial speed before and after the LC transition. In these experiments, a fluorophore (with an excitation wavelength in the blue) was used to visualize the bacteria, whereas our study was performed in brightfield microscopy. It is well established that atmospheric oxygen can react with fluorophores by photobleaching it. These reactions create reactive oxygen that can break lipid chains, thus compromising the membrane of the bacteria (58,59). We experimentally demonstrated (see Section S4) that the slow bacterial speed at DSCG concentrations below the LC transition (~4 μm/s, see Fig. S4 *C*), reported in Kumar et al. (2), was attributable to the effect of the reactive oxygen. Obviously, this effect can be inhibited by anaerobic conditions. As it takes at least 25 min (after the chamber is sealed) for DSCG aggregates to align, it is likely that the observations performed above the LC transition were done in the absence of oxygen (consumed by bacteria) (see Fig. S4 *D*). This would explain why the speed above the LC transition (~3 μm/s) is the same in both experiments.

Previous reports have shown that the motility of bacteria slows down when the oxygen is consumed in a solution containing glucose or stops if no glucose is present (60,61). However, we are not aware of any measurement of the influence of

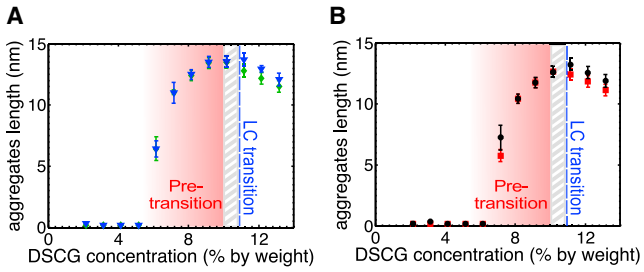

FIGURE 8 Estimation of the aggregates length computed with the Krieger and Dougherty model as a function of DSCG concentration. (*A*) The length of DSCG aggregates calculated from the viscosity of MB solution in the direction parallel (*triangles*) and perpendicular (*diamonds*) to **n**. (*B*) The length of DSCG aggregates calculated from the viscosity of DI water solution in the direction parallel (*squares*) and perpendicular (*dots*) to **n** (viscosity data taken from Duchesne et al. (27)). The gray hatched zone represents the DSCG concentration range where both phases coexist (isotropic and anisotropic). To see this figure in color, go online.

oxygen on the swimming speed of bacteria in a solution containing glucose. To quantify that relationship, we recorded the speed of bacteria swimming in MB containing glucose (or not) over long periods of time (2 h). The results are shown on Fig. 9. When no glucose is available, the bacteria run out of oxygen and stop swimming in less than 30 min. When glucose is present, bacteria can use it to carry out mixed acid fermentation and continue to swim in anaerobic conditions (for at least 2 h), albeit at a lower speed. From Fig. 9 *B* we note that the oxygenated speed is about two times higher than the speed when oxygen is exhausted (15 vs. 8 μm/s). These experiments were made with a high concentration of bacteria ($OD_{600} = 1$). When this concentration was decreased around the one used in DSCG experiments ($OD_{600} \sim 0.15$), the time before the complete exhaustion of oxygen greatly differed from sample to sample, varying from 15 min to more than 1 h. This phenomenon was probably caused by fluctuations in the starting oxygen concentration in each cell. Because all observations at DSCG concentrations below 11 wt % were made within 10 min, we are confident that we recorded oxygenated speeds for all concentrations below the LC transition. For the three higher concentrations in Fig. 2 *A*, our observations may have been made in anaerobic conditions and the equivalent oxygenated speed could have been up to twice as high. The asymmetric error bars on the last three points reflect that uncertainty.

Before concluding, we would like to discuss a couple of additional observations. First, by looking closely at the bacterial tracks (shown on Fig. 1 *B*), one observes a Brownian diffusion in the *y* axis (perpendicular to the director) similar to the one obtained with microspheres (Fig. 3 *B*). This indicates that the active machinery that allows the bacteria to swim (the flagella) acts almost exclusively in the direction parallel to the director (the *x* axis). The cell body is constrained (by the LC elastic forces) to maintain its long axis along the director **n**, as was also previously reported (4).

To ensure that the observed trajectories in the LC nematic phase were not the result of passive diffusion, we also tracked more than 100 nonmotile bacteria whose filaments were genetically removed. Because the trajectories of these nonmotile bacteria (Fig. 3 *C*) are qualitatively equivalent to those of microspheres (Fig. 3 *B*), we conclude that the anisotropic swimming behavior of active bacteria does not simply come from the elongated shape of their bodies. Therefore, we hypothesize that the filaments (thin helicoids long of several body lengths) should also be aligned with the director and push the bacteria in the direction of **n**. More research is needed on this topic, but it is very clear that the active displacement of bacteria is significantly different from the diffusion of microscopic objects in the same anisotropic environment.

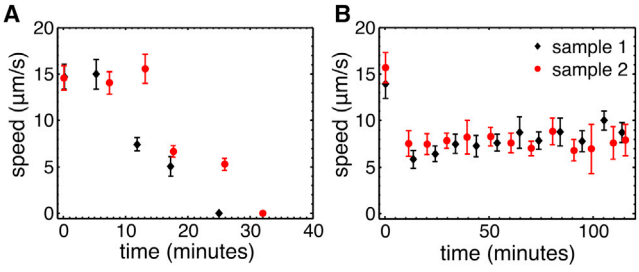

FIGURE 9 Effect of oxygen and glucose on the speed of bacteria in a closed chamber. (*A*) Speed of bacteria as a function of time in closed cells with a high bacterial concentration ($OD_{600} = 1$) in a MB without glucose and (*B*) with 0.02 M glucose. The SD was used as the error bars. To see this figure in color, go online.

Finally, although it is not affecting our key conclusions, we would like to address one discrepancy between the viscosity measurements reported in our study and the data we can find in the literature (4,30). Indeed, for a DSCG solution with a concentration of 15 wt % and a temperature of 25°C, the viscosity measured by a rheology method was found to be $\sim\eta = 1000\ \mathrm{g/(ms)}$ (4). This is to be compared with our values of $\eta_{\parallel} = (84 \pm 1)\mathrm{g/(ms)}$ and $\eta_{\perp} = (187 \pm 3)\mathrm{g/(ms)}$ at 13 wt %. The trend of our viscosity versus concentration plot in Fig. 4 *A* is reassuring because, for lower concentrations of the DSCG, our viscosity value is converging toward $\eta = 1\mathrm{g/(ms)}$, as it is expected for water (see also the calibration of this technique in Duchesne et al. (27) that confirms its accuracy). It is hard to believe, however, that the viscosity could increase by an order of magnitude between 13 and 15 wt % DSCG to reach the value $\eta = 1000\ \mathrm{g/(ms)}$. At this stage, we do not know yet the reason for this discrepancy, but our best hypothesis would be that this difference is caused by the different methods used. Indeed, it has previously been shown that the viscosity measured with rheology method in Sunset Yellow (another chromonic LC) could change by a factor of 2 when the shear rate is modified during the measurement (62). Other measurements turned out to be very sensitive to the particle surfaces and LC anchoring conditions (33,63,64).

CONCLUSIONS

Our study shows that the motility of bacteria in DSCG-water solutions (LC) is sensitive to the morphology and microstructure of the host. The combined effect of alignment of bacterial body (by elastic forces in the LC phase of the host) and of the anisotropic viscosity of the host (lower in the direction parallel to its anisotropy axis) favors its movement along linear traces. In addition to these pure elastic energy considerations, the strongly anisotropic viscosity of the host media should create an effective dynamic torque favoring the anisotropic swimming. These effects cannot, however, fully explain the behavior of the bacteria (like the reversals in direction), and the observation of the flagella movements should complete this explanation.

Our quantitative studies of the bacterial motility and of the diffusion of microspheres in DSCG solutions of various concentrations have uncovered the existence of a pretransition zone (between 6 and 10 wt %) where the DSCG-water

solution has not yet gone through its isotropic-anisotropic phase transition. In that zone, the viscosity of the medium is undergoing an exponential growth with DSCG concentration, the propulsive force of bacteria increases and their motility is strongly limited because they stick to each other and to surfaces. Based on the measured increase in the solution's viscosity and in the propulsive force, we think that the size of DSCG aggregates drastically increases in that pretransition zone. Because of that increase in aggregates size, it seems likely that the depletion effect becomes important in this zone and generates the observed sticking phenomenon in the isotropic phase of the medium. Our data suggest a threshold, at a concentration of ~6 $\pm$ 1 wt %, where the length of DSCG aggregates starts to increase rapidly.

It is interesting (almost ironic) to note that new physical properties of a material (exponential increase of viscosity, pretransition zone, etc.) were discovered by observing the behavior of bacteria, which are themselves not fully understood yet. At the same time, it shows that bacteria could be used as qualitative or even quantitative probes to detect physical properties in biocompatible media (such as aggregation, anisotropy, non-Newtonian fluid properties, etc.) This study reveals yet another layer of rich complexity in the physical characteristics of lyotropic LCs, which are bound to play an increasingly important role in our technologies thanks to their biocompatibility. Understanding the behavior of living microorganisms in these LCs promises to open extraordinary possibilities for further study of biological systems and the control of their movements. For example, we can imagine various applications in the areas of lab-on-a-chip (to control the bacteria movements) or of smart bandages where an anisotropic gel would force bacteria to move on the outskirts of the wound.

SUPPORTING MATERIAL

Supporting Materials and Methods, eleven figures, and four tables are available at http://www.biophysj.org/biophysj/supplemental/S0006-3495(15)01007-3.

AUTHOR CONTRIBUTIONS

I.D., S.R., and T.G. designed the experiments and wrote the manuscript. I.D. conducted all the experiments and analyses.

ACKNOWLEDGMENTS

We acknowledge the financial support of the Canada Foundation for Innovation (CFI), the Natural Sciences and Engineering Research Council of Canada (NSERC), and CREATE. T.G. thanks Canada Research Chair in Liquid Crystals and Behavioral Biophotonics and Manning Innovation price for financial support. We are grateful to G. Paradis, K. Allahverdyan, and Dr. A. Tork (from LensVector and TLCL Optical Research, Inc.) for their help during our experiments, to the group of H.C. Berg for bacterial strains, and to Remy Colin for sharing with us his tracking algorithm. We also acknowledge the important contribution of Wilson Poon for bringing the depletion mechanism to our attention and his other thoughtful comments on the manuscript.

SUPPORTING CITATIONS

References (65,66) appear in the Supporting Material.

REFERENCES

1. Smalyukh, I. I., J. Butler, …, G. C. L. Wong. 2008. Elasticity-mediated nematiclike bacterial organization in model extracellular DNA matrix. *Phys. Rev. E Stat. Nonlin. Soft Matter Phys.* 78:030701.
2. Kumar, A., T. Galstian, …, S. Rainville. 2013. The motility of bacteria in an anisotropic liquid environment. *Mol. Cryst. Liq. Cryst.* 574:33–39.
3. Zhou, S., A. Sokolov, …, I. S. Aranson. 2014. Living liquid crystals. *Proc. Natl. Acad. Sci. USA.* 111:1265–1270.
4. Mushenheim, P. C., R. R. Trivedi, …, N. L. Abbott. 2014. Dynamic self-assembly of motile bacteria in liquid crystals. *Soft Matter.* 10:88–95.
5. Mushenheim, P. C., R. R. Trivedi, …, N. L. Abbott. 2014. Using liquid crystals to reveal how mechanical anisotropy changes interfacial behaviors of motile bacteria. *Biophys. J.* 107:255–265.
6. Rey, A. D., E. E. Herrera-Valencia, and Y. K. Murugesan. 2014. Structure and dynamics of biological liquid crystals. *Liq. Cryst.* 41:430–451.
7. Viney, C., A. E. Huber, and P. Verdugo. 1993. Liquid crystalline order in mucus. *Macromolecules.* 26:852–855.
8. Viney, C. 1999. Mucus liquid crystallinity: is function related to microstructural domain size? *Biorheology.* 36:319–323.
9. Davies, J. M., and C. Viney. 1998. Water–mucin phases: conditions for mucus liquid crystallinity. *Thermochim. Acta.* 315:39–49.
10. Kupchinov, B. I., S. F. Ermako, …, V. N. Kestelman. 1993. Role of liquid crystals in the lubrication of living joints. *Smart Mater. Struct.* 2:7.
11. Nocton, J. J., F. Dressler, …, A. C. Steere. 1994. Detection of *Borrelia burgdorferi* DNA by polymerase chain reaction in synovial fluid from patients with Lyme arthritis. *N. Engl. J. Med.* 330:229–234.
12. Hughes, J. G., E. A. Vetter, …, F. R. Cockerill, 3rd. 2001. Culture with BACTEC Peds Plus/F bottle compared with conventional methods for detection of bacteria in synovial fluid. *J. Clin. Microbiol.* 39:4468–4471.
13. Hermanowicz, S., U. Schindler, and P. Wilderer. 1996. Anisotropic morphology and fractal dimensions of biofilms. *Water Res.* 30:753–755.
14. Van Wey, A. S., A. L. Cookson, …, P. R. Shorten. 2012. Anisotropic nutrient transport in three-dimensional single species bacterial biofilms. *Biotechnol. Bioeng.* 109:1280–1292.
15. Houry, A., M. Gohar, …, R. Briandet. 2012. Bacterial swimmers that infiltrate and take over the biofilm matrix. *Proc. Natl. Acad. Sci. USA.* 109:13088–13093.
16. Yeh, P., and C. Gu. 2010. Optics of Liquid Crystal Displays. John Wiley & Sons, Hoboken, NJ.
17. Galstian, T. V. 2013. Smart mini-cameras. CRC Press, Boca Raton, FL.
18. Tomilin, M. G., S. K. Stafeev, and A. Stepanova. 2006. Influenza viruses optical detection based on liquid crystals. *Proc. SPIE.* 6398:639813.
19. Shiyanovskii, S. V., O. D. Lavrentovich, …, K. J. Doane. 2005. Lyotropic chromonic liquid crystals for biological sensing applications. *Mol. Cryst. Liq. Cryst.* 434:259/[587]–270/[598].
20. Berg, H. C., and D. A. Brown. 1972. Chemotaxis in *Escherichia coli* analysed by three-dimensional tracking. *Nature.* 239:500–504.
21. Frymier, P. D., R. M. Ford, …, P. T. Cummings. 1995. Three-dimensional tracking of motile bacteria near a solid planar surface. *Proc. Natl. Acad. Sci. USA.* 92:6195–6199.

22. Molaei, M., M. Barry, …, J. Sheng. 2014. Failed escape: solid surfaces prevent tumbling of *Escherichia coli*. *Phys. Rev. Lett.* 113:068103.
23. Parkinson, J. S. 1978. Complementation analysis and deletion mapping of *Escherichia coli* mutants defective in chemotaxis. *J. Bacteriol.* 135:45–53.
24. Yuan, J., and H. C. Berg. 2010. Thermal and solvent-isotope effects on the flagellar rotary motor near zero load. *Biophys. J.* 98:2121–2126.
25. Lydon, J. 2011. Chromonic liquid crystalline phases. *Liq. Cryst.* 38:1663–1681.
26. Seo, D. S., H. Matsuda, …, S. Kobayashi. 1993. Alignment of nematic liquid crystal(5CB) on the treated substrates: characterization of orientation films, generation of pretilt angles, and surface anchoring strength. *Mol. Cryst. Liq. Cryst.* 224:13–31.
27. Duchesne, I., S. Rainville, and T. Galstian. 2015. Application of a microrheology technique to measure the viscosity of disodium cromoglycate liquid crystal. *Mol. Cryst. Liq. Cryst.*, Submitted.
28. de Gennes, P. G., and J. Prost. 1995. The Physics of Liquid Crystals. Clarendon Press, New York.
29. Saveyn, H., B. De Baets, …, P. Van der Meeren. 2010. Accurate particle size distribution determination by nanoparticle tracking analysis based on 2-D Brownian dynamics simulation. *J. Colloid Interface Sci.* 352:593–600.
30. Turiv, T., I. Lazo, …, O. D. Lavrentovich. 2013. Effect of collective molecular reorientations on Brownian motion of colloids in nematic liquid crystal. *Science.* 342:1351–1354.
31. Berezhkovskii, A. M., L. Dagdug, and S. M. Bezrukov. 2014. Discriminating between anomalous diffusion and transient behavior in microheterogeneous environments. *Biophys. J.* 106:L09–L11.
32. Purcell, E. M. 1977. Life at low Reynolds number. *Am. J. Phys.* 45:3–11.
33. Stark, H., and D. Ventzki. 2001. Stokes drag of spherical particles in a nematic environment at low Ericksen numbers. *Phys. Rev. E Stat. Nonlin. Soft Matter Phys.* 64:031711.
34. Ryzhkova, A. V., and I. Muševič. 2013. Particle size effects on nanocolloidal interactions in nematic liquid crystals. *Phys. Rev. E Stat. Nonlin. Soft Matter Phys.* 87:032501.
35. Nastishin, Y. A., H. Liu, …, M. A. Anisimov. 2004. Pretransitional fluctuations in the isotropic phase of a lyotropic chromonic liquid crystal. *Phys. Rev. E Stat. Nonlin. Soft Matter Phys.* 70:051706.
36. Smalyukh, I. I., O. D. Lavrentovich, …, P. N. Prasad. 2005. Elasticity-mediated self-organization and colloidal interactions of solid spheres with tangential anchoring in a nematic liquid crystal. *Phys. Rev. Lett.* 95:157801.
37. Poulin, P., and D. A. Weitz. 1998. Inverted and multiple nematic emulsions. *Phys. Rev. E Stat. Nonlin. Soft Matter Phys.* 57:626–637.
38. Sowa, Y., and R. M. Berry. 2008. Bacterial flagellar motor. *Q. Rev. Biophys.* 41:103–132.
39. Martinez, V. A., J. Schwarz-Linek, …, W. C. K. Poon. 2014. Flagellated bacterial motility in polymer solutions. *Proc. Natl. Acad. Sci. USA.* 111:17771–17776.
40. Darnton, N. C., L. Turner, …, H. C. Berg. 2007. On torque and tumbling in swimming *Escherichia coli*. *J. Bacteriol.* 189:1756–1764.
41. Berg, H. C., and L. Turner. 1979. Movement of microorganisms in viscous environments. *Nature.* 278:349–351.
42. Schneider, W. R., and R. N. Doetsch. 1974. Effect of viscosity on bacterial motility. *J. Bacteriol.* 117:696–701.
43. Magariyama, Y., and S. Kudo. 2002. A mathematical explanation of an increase in bacterial swimming speed with viscosity in linear-polymer solutions. *Biophys. J.* 83:733–739.
44. Nakamura, S., Y. Adachi, …, Y. Magariyama. 2006. Improvement in motion efficiency of the spirochete *Brachyspira pilosicoli* in viscous environments. *Biophys. J.* 90:3019–3026.
45. Atsumi, T., Y. Maekawa, …, M. Homma. 1996. Effect of viscosity on swimming by the lateral and polar flagella of *Vibrio alginolyticus*. *J. Bacteriol.* 178:5024–5026.
46. Mao, Y., M. E. Cates, and H. N. W. Lekkerkerker. 1997. Theory of the depletion force due to rodlike polymers. *J. Chem. Phys.* 106:3721–3729.
47. Yaman, K., C. Jeppesen, and C. M. Marques. 1998. Depletion forces between two spheres in a rod solution. *Europhys. Lett.* 42:221.
48. Schwarz-Linek, J., G. Dorken, …, W. C. K. Poon. 2010. Polymer-induced phase separation in suspensions of bacteria. *Europhys. Lett.* 89:68003.
49. Dorken, G., G. P. Ferguson, …, W. C. K. Poon. 2012. Aggregation by depletion attraction in cultures of bacteria producing exopolysaccharide. *J. R. Soc. Interface.* 9:3490–3502.
50. Rubio-Hernández, F. J., M. F. Ayúcar-Rubio, …, F. J. Galindo-Rosales. 2006. Intrinsic viscosity of SiO_2, Al_2O_3 and TiO_2 aqueous suspensions. *J. Colloid Interface Sci.* 298:967–972.
51. Kovalchuk, N., V. Starov, and R. Holdich. 2010. Effect of aggregation on viscosity of colloidal suspension. *Colloid J.* 72:647–652.
52. Barthelmes, G., S. E. Pratsinis, and H. Buggisch. 2003. Particle size distributions and viscosity of suspensions undergoing shear-induced coagulation and fragmentation. *Chem. Eng. Sci.* 58:2893–2902.
53. Duan, F., D. Kwek, and A. Crivoi. 2011. Viscosity affected by nanoparticle aggregation in Al_2O_3-water nanofluids. *Nanoscale Res. Lett.* 6:248.
54. Krieger, I. M., and T. J. Dougherty. 1959. A mechanism for non-Newtonian flow in suspensions of rigid spheres. *Trans. Soc. Rheol.* 3:137–152.
55. Dickinson, A. J., N. D. LaRacuente, …, P. J. Collings. 2009. Aggregate structure and free energy changes in chromonic liquid crystals. *Mol. Cryst. Liq. Cryst.* 509:9/[751]–20/[762].
56. Hartshorne, N. H., and G. D. Woodard. 1973. Mesomorphism in the system disodium chromoglycate-water. *Mol. Cryst. Liq. Cryst.* 23:343–368.
57. Tanford, C. 1961. Physical Chemistry of Macromolecules. Wiley and Sons, New York.
58. Hadjur, C., N. Lange, …, G. Wagnières. 1998. Spectroscopic studies of photobleaching and photoproduct formation of *meta*(tetrahydroxyphenyl)chlorin (*m*-THPC) used in photodynamic therapy. The production of singlet oxygen by *m*-THPC. *J. Photochem. Photobiol. B.* 45:170–178.
59. Heiser, I., W. Oswald, and E. F. Elstner. 1998. The formation of reactive oxygen species by fungal and bacterial phytotoxins. *Plant Physiol. Biochem.* 36:703–713.
60. Adler, J., and B. Templeton. 1967. The effect of environmental conditions on the motility of *Escherichia coli*. *J. Gen. Microbiol.* 46:175–184.
61. Douarche, C., A. Buguin, …, A. Libchaber. 2009. *E. coli* and oxygen: a motility transition. *Phys. Rev. Lett.* 102:198101.
62. Prasad, S. K., G. G. Nair, …, V. Jayalakshmi. 2007. Evidence of wormlike micellar behavior in chromonic liquid crystals: rheological, x-ray, and dielectric studies. *J. Phys. Chem. B.* 111:9741–9746.
63. Senyuk, B., D. Glugla, and I. I. Smalyukh. 2013. Rotational and translational diffusion of anisotropic gold nanoparticles in liquid crystals controlled by varying surface anchoring. *Phys. Rev. E Stat. Nonlin. Soft Matter Phys.* 88:062507.
64. Koenig, G. M., Jr., R. Ong, …, N. L. Abbott. 2009. Single nanoparticle tracking reveals influence of chemical functionality of nanoparticles on local ordering of liquid crystals and nanoparticle diffusion coefficients. *Nano Lett.* 9:2794–2801.
65. Purcell, E. M. 1997. The efficiency of propulsion by a rotating flagellum. *Proc. Natl. Acad. Sci. USA.* 94:11307–11311.
66. Chattopadhyay, S., R. Moldovan, …, X. L. Wu. 2006. Swimming efficiency of bacterium *Escherichia coli*. *Proc. Natl. Acad. Sci. USA.* 103:13712–13717.

Supporting Material

Bacterial Motility Reveals Unknown Molecular Organization

Ismaël Duchesne, Simon Rainville and Tigran Galstian*

*Department of Physics, Engineering Physics and Optics and Center for Optics, Photonics and Lasers, Laval University, Quebec City, Canada G1V 0A6

S1 Linear correlation between the mean squared displacement (MSD) and the time

The diffusion of particles in a liquid crystal (LC) can be in normal or anomalous regimes depending upon the time scale used to record their movements [1, 2]. The anomalous behavior is characterized by a non-linear relation between the mean squared displacement (MSD) and time, whereas the normal diffusion corresponds to a linear relationship. By plotting the MSD for our viscosity measurements as a function of time, we obtained a linear relation at every concentration, which indicates normal diffusion [3]. To quantify this linear relationship, we computed the linear correlation coefficient (also known as the Pearson product-moment coefficient of correlation) of the relation between the MSD and the time for a short period of time (10 first frames) and for a longer period (50 first frames). As we can see in Fig. S1, the coefficient is always very close to 1, which mean a very good linear relation. This result is in agreement with [3] where normal diffusion was also obtained for the same time scale (minimum sample rate of 0.4 s) but with DSCG solution in deionized water.

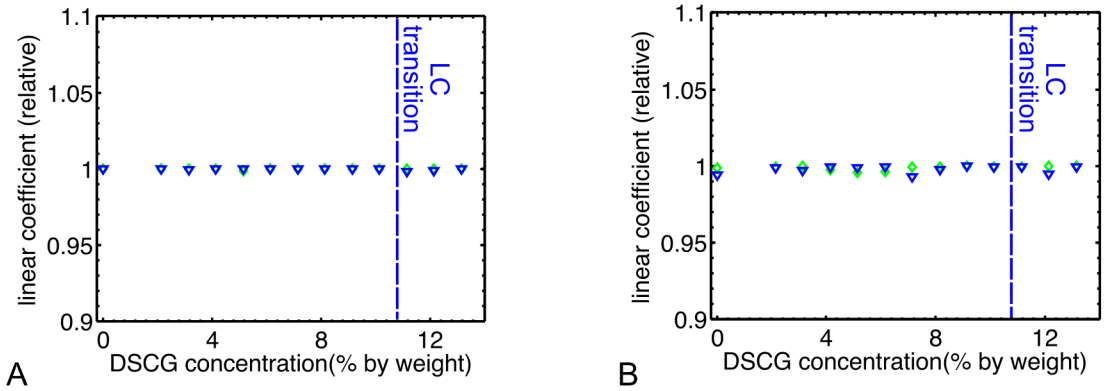

Figure S1: Linear coefficient of the mean squared displacement vs time showing that the diffusion is normal (at every DSCG concentration). (A) Linear coefficient computed from the first 10 data points and (B) from the first 50 data points. The green diamonds were calculated from the viscosity parallel to $\mathbf{n}$ and the blue triangles from the viscosity perpendicular to $\mathbf{n}$. At each concentration, the probability to obtain the same coefficient value with a random distribution was estimated to be $\leq 10^{-16}$.

S2 Propulsive force and variable torque regime

The flagellar motor of the bacteria can work in two regimes [4]. The first one appears when the motor rotates at low angular speed, below the critical angular speed ω_m^c (see Fig. S2*A*). In this regime, the torque of the motor remains constant when its angular speed changes. Thus, the torque applied by the motor is not modified when the load (here, the viscosity of the medium) changes. In the second regime, when the motor rotates at an angular speed higher than ω_m^c, the torque decreases linearly with increasing angular speed until it becomes 0 when the maximum angular speed (ω_m^{max}) is reached. Consequently, the torque produced by the motor increases when the load (or viscosity) is raised. This section will show that the torque increase cannot explain the increase in the propulsive force in the pretransition zone and in the anisotropic phase, even if both the constant and variable regimes seem to be present in our experiments.

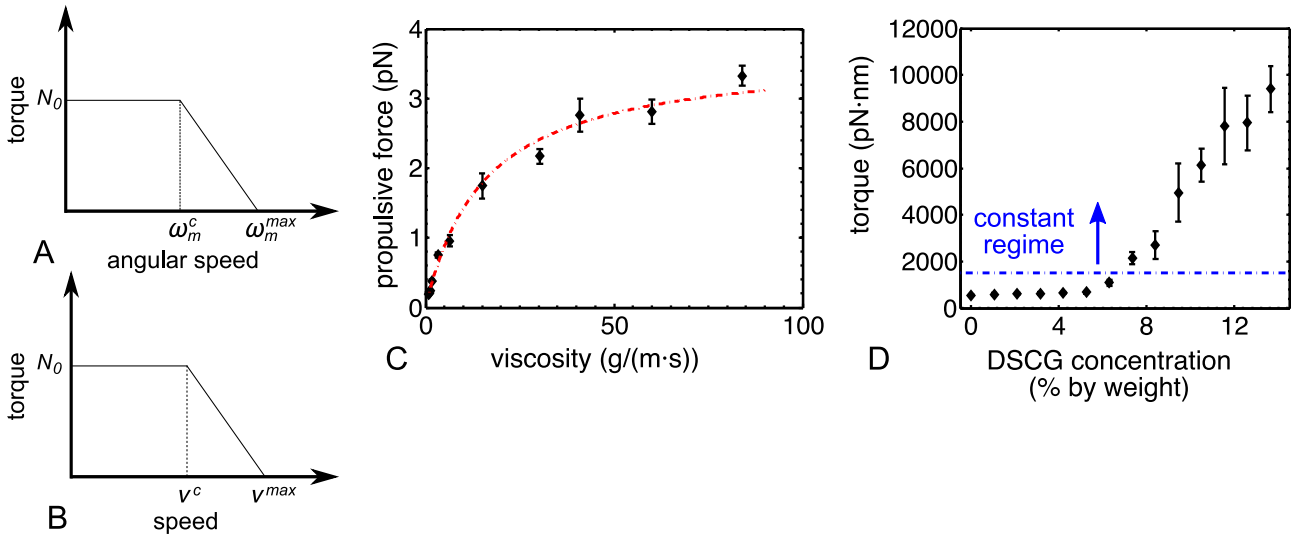

Figure S2: Relationship between the torque (exerted by the motor), the angular speed of the motor and the speed of the bacteria. (*A*) Schematic of the torque produced by the motor on its angular speed and (*B*) on the speed of the bacteria. (*C*) Estimation of the propulsive force produced by the bacteria as a function of the viscosity of the DSCG solutions. (*D*) Equivalent stall torque (N_0) as a function of the DSCG concentration computed with the propulsive force in *C* by considering a constant torque regime. The dotted line in *C* represents the best fit of the propulsive force computed by using the Purcell's model in the variable torque regime (Eq. S12). The average known stall torque N_0 for *E. coli* is shown with the dotted line in *D* [4,5].

The Purcell's model describes the forces involved when a bacterium swims in a Newtonian liquid. In this model, the bacterium is described by a prolate spheroid and it has only one filament at one of its poles. The forces and the torques on the body and the filament are described by [5,6]

$$F_b = -A_0 v, \tag{S1}$$

$$N_b = -D_0 \Omega, \tag{S2}$$

$$F_f = -Av - B\omega \tag{S3}$$

and

$$N_f = -Bv - D\omega, \tag{S4}$$

where v is the speed of the bacterium, Ω is the angular speed of the body, ω is the angular speed of the filament (negative), and A_0, D_0, A, B and D depend linearly on the viscosity. Since the total force and

torque must be zero for a stationary movement of bacterium (no external forces applied), we can solve these equations to obtain the relation between the speed, ω and Ω [5]:

$$v = \frac{B}{A_0 + A}\omega \equiv \gamma\omega, \tag{S5}$$

$$v = \frac{D(A_0 + A) - B^2}{D_0 B}\Omega \equiv R_1\Omega, \tag{S6}$$

where γ and R_1 are independent of the viscosity. The angular speed of the motor is given by the addition of the rotations of the body and the filament. With the equations above we obtain a relation between the angular speed of the motor and the speed of the bacterium:

$$\omega_m = \omega + \Omega = (\gamma^{-1} + R_1^{-1})v. \tag{S7}$$

We can see that the speed of the bacterium and the angular speed of the motor are two equivalent quantities that are proportional to each other. Thus, the relationship between the torque and the speed of the bacterium comprises the same two regimes mentioned above for the angular speed of the motor (see Fig. S2B). From Eq. S6 above and Eqs. 10a and 10b from [5] we obtain the dependence of the speed on the viscosity for the two regimes of torque (constant or variable):

$$\text{if } \omega_m < \omega_m^c\,, \quad v = \frac{N_0}{D_0 R_1} \equiv \frac{N_0}{d_0 R_1 \eta}, \tag{S8}$$

$$\text{if } \omega_m > \omega_m^c\,, \quad v = \frac{\alpha_v v^{max}}{D_0 R_1 + \alpha_v} \equiv \frac{\alpha_v v^{max}}{d_0 R_1 \eta + \alpha_v}, \tag{S9}$$

where

$$\alpha_v = \left|\frac{dN}{dv}\right| = \frac{N_0}{v^{max} - v^c}, \tag{S10}$$

$D_0 = \frac{16\pi\eta ab^2}{3}$ with a and b being the semi-major and semi-minor axes of the prolate spheroid, N_0 is the stall torque and $d_0\eta = D_0$. In the two regimes, the drag force (used as the approximation of the propulsive force) on the body of the bacteria (Eq. S1) becomes

$$\omega_m < \omega_m^c: \quad F_b = A_0\frac{N_0}{D_0 R_1} \equiv \frac{a_0 N_0}{d_0 R_1}, \tag{S11}$$

$$\omega_m > \omega_m^c: \quad F_b = A_0\frac{\alpha_v v^{max}}{D_0 R_1 + \alpha_v} \equiv \frac{a_0\alpha_v v^{max}}{d_0 R_1 + \alpha_v \eta^{-1}}, \tag{S12}$$

where $a_0\eta = A_0$. As we can see, the propulsive force does not depend on the viscosity in the low speed regime, but it does in the high speed regime. The values of the constants in the above equations are:

$$A = k_n L \sin\Psi \tan\Psi(1 + \gamma\cot^2\Psi)\eta, \tag{S13}$$

$$B = k_n L\frac{\lambda}{2\pi}\sin\Psi\tan\Psi(1 - \gamma)\eta, \tag{S14}$$

$$D = k_n L\left(\frac{\lambda}{2\pi}\right)^2\sin\Psi\tan\Psi(1 + \gamma\cot^2\Psi)\eta, \tag{S15}$$

$$A_0 = \frac{4\pi a}{\ln\frac{2a}{b} - \frac{1}{2}}\eta, \tag{S16}$$

$$D_0 = \frac{16\pi}{3}ab^2\eta, \tag{S17}$$

with

$$k_n = \frac{8\pi}{2\ln\frac{c\lambda}{r} + 1}, \tag{S18}$$

$$k_t = \frac{4\pi}{2\ln\frac{c\lambda}{r} - 1}, \tag{S19}$$

where $L = 7\,\mu$m is the length of the filament, $\Psi = 41\,^\circ$ is the angle made by the flagellar filament with the flagellar axis, $\gamma = \frac{k_t}{k_n}$, $\lambda = 2\,\mu$m is the pitch of the filament, $r = 20\,$nm is the estimated radius of the tube that composed the filament and $c = 2.4$ is the Lighthill constant [5, 7].

As we can see in Fig. S2*C* the propulsive force increases when the viscosity of the DSCG solution is raised. To find out whether this increase in the propulsive force is caused by the increase of the torque exerted by the motor, we draw the equivalent stall torque N_0 for each DSCG concentration using the constant torque regime equation (Eq. S11). The value of N_0 varies from $550 \pm 26\,\mathrm{pN \cdot nm}$ to $9400 \pm 980\,\mathrm{pN \cdot nm}$ (see Fig. S2*D*). From [4,5], N_0 should be around $1500\,\mathrm{pN \cdot nm}$ for *E. coli*, so the constant regime should be reached between 6.2 wt% and 7.2 wt% (see the blue line in Fig. S2*D*). Therefore the torque of the bacteria should be variable only for the concentrations below 7.2 wt% and the propulsive force should be constant at concentrations above. Furthermore, the increase in the torque of the bacteria cannot explain why N_0 reaches $9000\,\mathrm{pN \cdot nm}$ at high DSCG concentration, a value far away from the known N_0 for *E. coli* (around $1500\,\mathrm{pN \cdot nm}$).

To complete our analysis, we fitted the dependence of the propulsive force on the viscosity with Eq. S12 (dotted line in Fig. S2*C*) by using $N_0 = 1500\,\mathrm{pN \cdot nm}$. The model correlates very well with our data when $v^c = 13.6 \pm 0.4\,\mu$m/s and $v^{max} = 15.9 \pm 0.5\,\mu$m/s. Here again, the torque should be variable only above a speed of $v^c = 13.6 \pm 0.4\,\mu$m/s, which correspond to a DSCG concentration below 8.2 wt% (see Fig. 2*A* of the paper). By using Eq. S7, we computed the equivalent angular speed of the motor and obtained $\omega_m^c = 61 \pm 2\,$Hz and $\omega_m^{max} = 71 \pm 2\,$Hz. These values are far away from known values with $\omega_m^c \sim 150\,$Hz and $\omega_m^{max} \sim 300\,$Hz [4]. Consequently, the variable torque cannot explain the increase in the propulsive force observed in the pretransition zone and anisotropic phase.

In summary, the variable torque regime could explain the increase in the propulsive force only below a DSCG concentration of 7.2 wt%, namely at the beginning of the pretransition zone and before. The additional increase of the propulsive force must be caused by another phenomenon. We think that, in the pretransition zone and anisotropic phase, the solution becomes highly non-Newtonian and this is why the Purcell's model cannot explain the increase of the propulsive force. The presence of the non-Newtonian medium would increase the propulsive force by increasing its efficiency (see paper for more information).

S3 Estimation of the depletion force in the pretransition zone

In a solution of large particles with much smaller rods with a diameter D and a length L, the depletion effect can cause the aggregation of the large particles. At first order in rods concentration, in the particular case where the particles are spheres of radius R and $D \ll L \ll R$, the depletion energy between two spheres is described by [8, 9]

$$U(h) = \frac{\pi k_B T n_r R L^2}{6} \left(\frac{h}{L} - 1 \right)^3, \tag{S20}$$

where k_B is the Boltzmann constant, T the temperature in Kelvin, n_r the number density of the rods and h is the distance between the surface of the spheres. This equation holds only for $0 \leq h \leq L$ since there is no depletion effect when the distance between the spheres is larger than L. Experimentally, we observed that bacteria are sometimes able to detach themselves from aggregates of bacteria or surfaces in the pretransition zone. We thus suppose that the phenomenon responsible for the sticky effect can apply a force similar to the propulsive force. To compare the strength of the depletion effect and of the propulsive force of the bacteria, the depletion force was derived from Eq. S20 :

$$F_d(h) = \frac{dU(h)}{dh} = \frac{\pi k_B T n_r R L}{2} \left(\frac{h}{L} - 1 \right)^2. \tag{S21}$$

Table S1: Measured and computed volume concentration and characteristics of DSCG solutions.

Concentration (± 0.2) (wt %)	Measured concentration (vol %)	Computed concentration (vol %)	Number density (10^{24} rods/m^3)	Aggregates length (nm)
0	0	0	—	—
2.2	1.4 ± 0.2	1.36	—	—
3.2	2.0 ± 0.3	2.00	—	—
4.2	2.7 ± 0.3	2.64	—	—
5.2	3.3 ± 0.3	3.29	—	—
6.2	3.9 ± 0.3	3.94	3.9 ± 0.5	6 ± 1
7.2	4.6 ± 0.4	4.60	2.7 ± 0.3	11.0 ± 0.4
8.2	5.2 ± 0.4	5.27	2.7 ± 0.3	12.4 ± 0.7
9.2	5.8 ± 0.5	5.93	2.8 ± 0.3	13.4 ± 0.7
10.2	6.5 ± 0.5	6.61	3.1 ± 0.3	13.5 ± 0.7
11.2	7.1 ± 0.5	7.29	3.7 ± 0.3	12.8 ± 0.7
12.2	7.7 ± 0.6	7.97	4.2 ± 0.4	12.2 ± 0.7
13.2	8.4 ± 0.6	8.66	4.8 ± 0.4	11.5 ± 0.7

To compute this force, we used $T = 295.65\,\mathrm{K}$ and the stokes radius of the bacteria as the radius of the sphere $R = 0.57 \pm 0.2\,\mu\mathrm{m}$ (see Eq. 8 of the paper). To obtain the number density of the rods we first measured the volume concentration of the DSCG molecules by comparing the motility buffer volume added to the solution to obtain the right weight concentration with the total volume of the final solution (see Table S1). The number density of the DSCG molecules was then computed with the following expression

$$n_{DSCG} = \frac{M_{DSCG} N_A}{M_w V_{tot}}, \tag{S22}$$

where M_{DSCG} is the mass of the DSCG in a given solution of total volume V_{tot}, N_A is the Avogadro constant and M_w is the molecular weight of the DSCG (512.33 g/mol). Finally to convert the number

density of molecules in terms of the number density of rods, we used the aggregation model presented in the paper. Indeed, each rod is made of a stack of disks with a thickness t_r of 0.34 nm and composed of two DSCG molecules. Thus, the equation below gives the number density of rods

$$n_r = \frac{n_{DSCG} t_r}{2L}. \tag{S23}$$

To verify whether our volume concentrations were consistent with the DSCG model described in the paper, we computed the theoretical volume fraction by using this model. For this purpose, the following expressions were used:

$$V_{H_2O} = \frac{M_{H_2O}}{\rho_{H_2O}}, \tag{S24}$$

$$V_{mol} = \frac{\pi r^2 L}{2}, \tag{S25}$$

$$N_{DSCG} = \frac{M_{DSCG} N_A}{M_w}, \tag{S26}$$

$$V_{DSCG} = N_{DSCG} V_{mol}, \tag{S27}$$

where M_{H_2O} is the mass of water in a solution, ρ_{H_2O} is the density of water, V_{mol} is the volume of one molecule of DSCG, r is the radius of the DSCG disk, N_{DSCG} is the number of DSCG molecules in the solution and V_{DSCG} is the volume occupied by the DSCG molecules in the solution. By comparing the theoretical results with our measurements (see Table S1) we can see that the difference between these two quantities is always $\leq 3.5\,\%$. Therefore, the model seem to be in good agreement with our measurements.

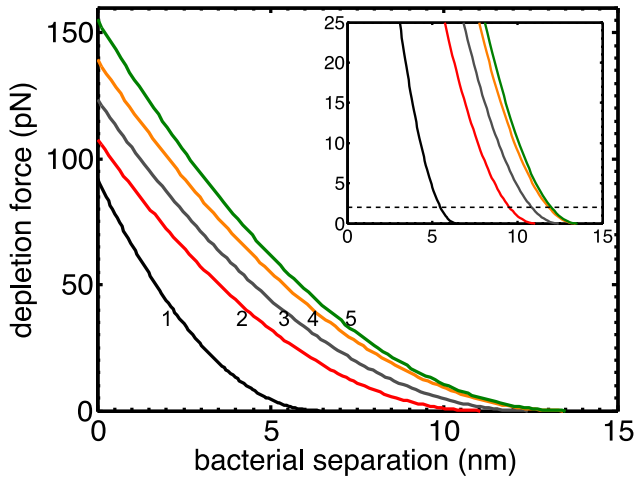

Figure S3: Estimated depletion force between two bacteria as a function of the distance between their surfaces. Each curve represents a different rod concentration: from left (1) to right (5), the concentration starts at 6.2 wt% and finishes at 10.2 wt% with an increment of 1 wt%. The dotted line in the inset shows the approximate value of the propulsive force in the pretransition zone (around 2 pN).

In Fig. S3 we can see the depletion force between two bacteria as a function of the distance between their surfaces for a DSCG concentration between 6.2 wt% and 10.2 wt%. By observing the maximal depletion force at each concentration, we observe that the strength of the depletion increases with concentration, which could explain why the bacteria become more and more sticky when the concentration is raised. Moreover, the depletion effect could be important in the sticky process of the bacteria since the maximum depletion force is always higher than the propulsive force of the bacteria in the pretransition zone (around 35 times higher at 6.2 wt% and 75 times higher at 10.2 wt%). This aspect could explain why the bacteria generally

remain stuck to surfaces or others bacteria in this zone. On the other hand, some bacteria are observed to detach themselves from aggregates of bacteria or others surfaces, and it is hard to believe that the propulsive force could reach a value as high as the maximum depletion force (even in the case where the propulsion of the two bacteria adds up). Indeed we can see in the inset of Fig. S3 the minimum distance between two bacteria where they are able to detach themselves using their propulsion only. This distance is around 5 nm at 6.2 wt% and 12 nm at 9.2 wt%. In is thus possible that the filament could momentarily create a perturbation in the depletion force, which could cause one bacterium to move a few nanometers away from the other, allowing it to detach. Furthermore, bacteria have many proteins that partially emerge from their membrane, and create some protuberance on their surface (on the nm scale). The surface of two bacteria (or one bacterium and the wall of the chamber) are probably never completely in contact, causing the depletion force to be smaller than the one computed.

We conclude that the depletion effect could explain the sticky behavior observed in the pretransition zone.

S4 Effect of reactive oxygen on the speed of the bacteria

When a fluorophore is exposed to light in the presence of atmospheric oxygen (O_2), it looses its fluorescence with time (photobleaching). This reaction creates reactive oxygen, for example singlet oxygen ($^1O_2$) and superoxide [10, 11]. These reactive forms will perturb the viability of the bacteria cell by breaking the proteins, DNA or lipid chains. To verify whether this effect can explain the discrepancy between our speed measurements and the speed obtained in [12], we recorded movies of swimming bacteria while they were exposed to light with and without fluorophore. To do so, a X-cite 120LED (Lumen dynamic, ON, Canada) with a blue filter at 482 nm (bandwidth of 35 nm) was used to illuminate the sample. The first experiments were made in motility buffer in presence of oxygen and the second, after the bacteria had consumed all the oxygen. As we can see on Fig. S4 *A* and *B*, the bacteria in both solutions do not seem to be sensitive to light. In contrast, when 0.01 mM of Syto 9 (from the Invitrogen Live Dead kit, the same fluorophore used in [12]) is added to the solution, the speed of the bacteria in an oxygenated solution decreases with increasing light intensity (see Fig. S4*C*). On the other hand, the bacteria in solution without oxygen remain unaffected by light (see Fig. S4*D*). Furthermore, in solutions with a higher concentration of bacteria, they seem to be less sensitive to the light. This could be caused by the fact that, at the moment of the experiments, the bacteria had consumed more oxygen, and also because the fluorophore concentration was higher in the concentrated bacteria solutions. Indeed, the fluorescence signal intensity from the bacteria in diluted samples was larger (at the same intensity of light).

These observations confirm that the reactive oxygen created by the presence of fluorophore compromises the motility of bacteria. As expected when we applied the same experimental condition used in [12] (0.01 mM SYTO 9 and OD 0.4), the speed of the bacteria in solution with oxygen slows down to around $4\,\mu$m/s before stopping. Furthermore, the motility of bacteria is not affected by light when all oxygen is exhausted in the chamber. This phenomenon explains why the speed of the bacteria in the isotropic phase (in presence of oxygen) differs in the two experiments and also, why the speed of the bacteria in the anisotropic phase (in absence of oxygen) is similar in both publications.

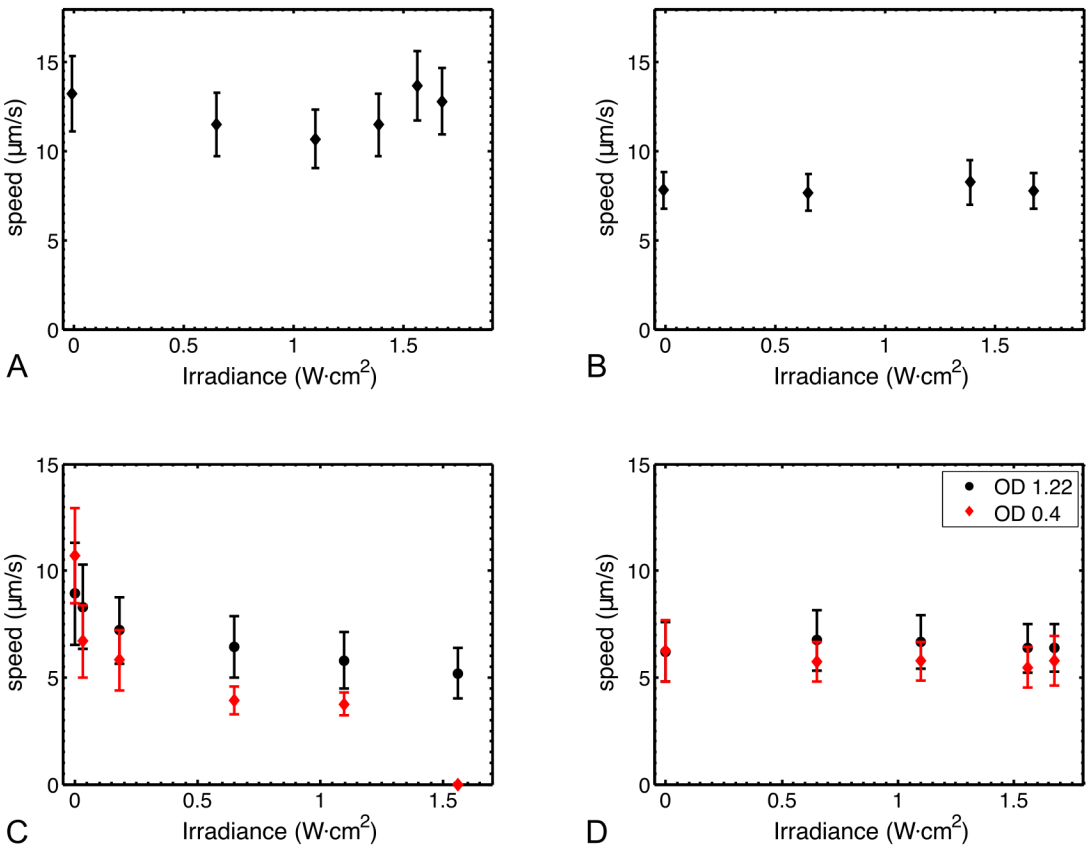

Figure S4: Effect of the reactive oxygen on the speed of the bacteria. Bacterial speed as a function of light intensity in motility buffer (A) with and (B) without the presence of oxygen. Bacterial speed as a function of the intensity of the light in motility buffer with 0.01 mM of Syto 9 (C) with and (D) without the presence of oxygen. Two sets of measurements are presented in C and D, one at high bacterial concentration (red diamonds) and the other at lower bacterial concentration. All experiments were performed at $22.5 \pm 0.5\,^{\circ}\mathrm{C}$.

S5 Typical Images

S5.1 Pretransition zone

This section shows bright field images of bacteria swimming in DSCG solutions (in motility buffer) in the pretransition zone. In each sequence, the images taken between parallel polarizers are all shown with the same intensity scale (the intensity scale is at the bottom right of the first image of each sequence). It is important to note that the images taken between crossed polarizers are shown with a different intensity scale to highlight how uniform these images are. The angle between the first polarizer and the x axis is reported on top of each image. The birefringence of our objective was corrected (in images taken between crossed polarizers) by using a sample at 0 wt % as calibration. All experiments were made at $22.5 \pm 0.5\,^{\circ}$C.

To quantify the isotropy of the LC samples in the pretransition zone (and rule out the presence of nematic domains), the extinction ratio was compared between images from the pretransition zone and the nematic phase. To do so, the intensity of each pixel of an image taken between parallel polarizers was divided by the intensity of images taken between perpendicular polarizers. The average and minimum extinction ratio r_e are reported in Table S2. The values in the pretransition zone are similar to those of the solution at 0 wt%. However, the minimum extinction ratio obtained in an inhomogeneous solution (at 10.2 wt%, see Fig. S8) is much smaller than those computed in the pretransition zone. Since this smaller minimum extinction ratio is caused by the presence of non-aligned nematic domains (see Fig. S8), this difference demonstrates that no small nematic domains are present in the pretransition zone. Furthermore, by observing the images taken between crossed polarizers in Figs. S5 and S7, no nematic domain can be seen (no bright zone similar to Fig. 3 *D* and *F* of the paper can be found in any image). We conclude that our solutions were always isotropic and homogeneous in the pretransition zone.

Table S2: Extinction ratio r_e of DSCG samples with bacteria. Extinction ratio, from 0 wt% to 9.2 wt% of DSCG, calculated with polarizer axis at 0° and 45° were similar, so we averaged their values.

Concentration (±0.2) (wt %)	Angle of the polarizer	r_e mean	r_e min
0	0° and 45°	15.5	11.0
7.2	0° and 45°	13.8	8.7
8.2	0° and 45°	16.0	9.8
9.2	0° and 45°	15.0	8.3
10.2	0°	11.2	1.7
10.2	45°	6.4	1.2
13.2	0°	12.2	2.3
13.2	45°	2.0	0.44

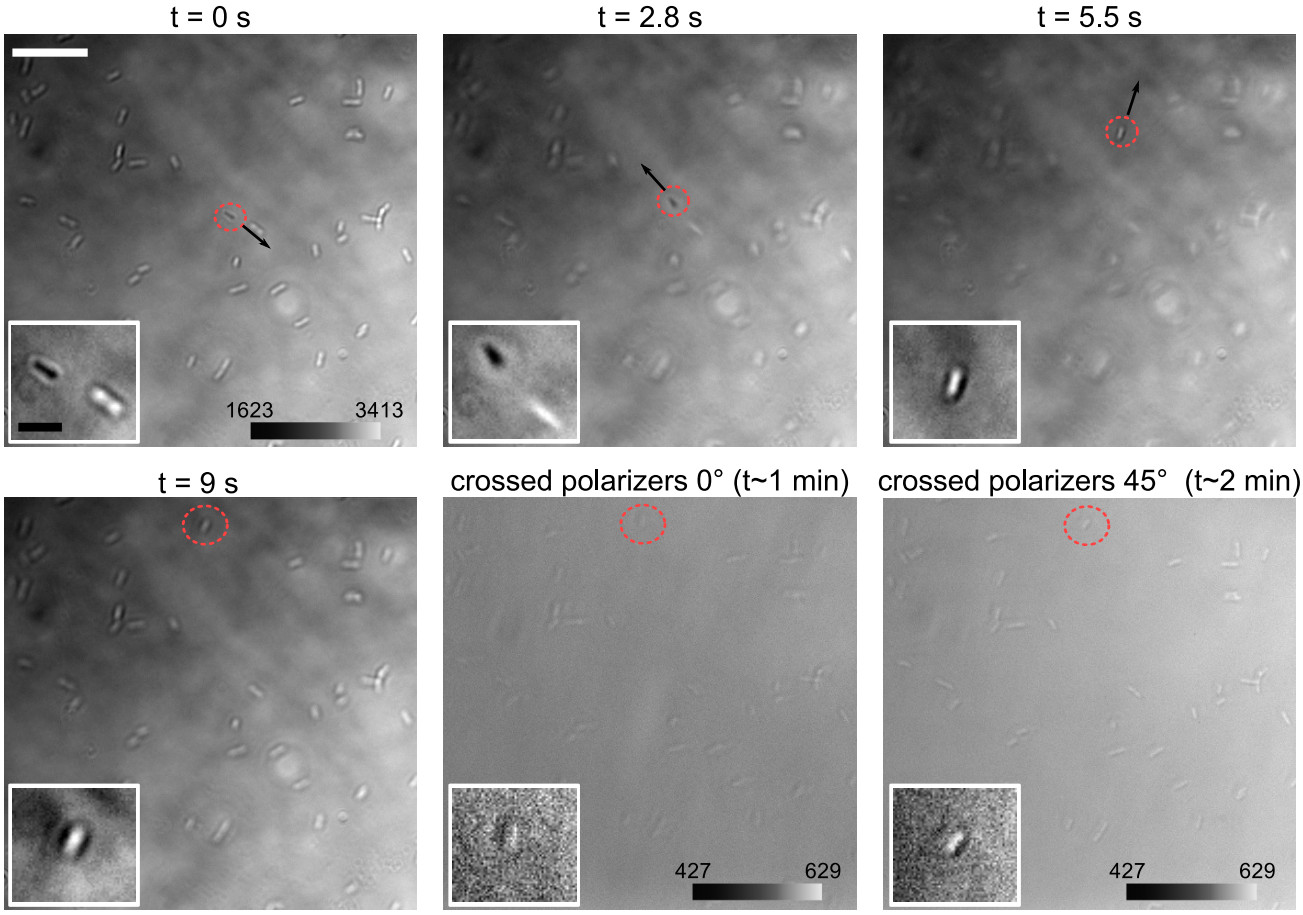

Figure S5: Sequence of images taken from a sample of bacteria with 7.2 wt% of DSCG. The sequence shows a swimming bacterium (circled in red) that remains stuck to the wall of the chamber at $t = 9\,\mathrm{s}$. The zoom of the region close to the swimming bacterium is shown (with enhanced contrast) in the white box at the bottom left of each image. Note that the movement of the bacterium in the z axis can be observed by the color of its body (black is further from the surface and white nearer). The first four images were taken between parallel polarizers (oriented at 0° from the x axis). The white scale bar (top left of the first image) measures $20\,\mu\mathrm{m}$ and the black bar (inset in the first image) measures $5\,\mu\mathrm{m}$.

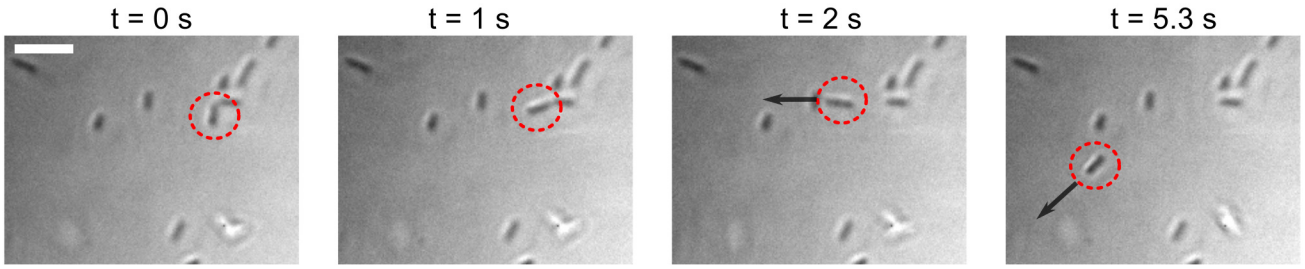

Figure S6: Sequence of images taken from a sample of bacteria with 7.2 wt% of DSCG showing the escape of a bacterium (circled in red) from an aggregate. All images were taken between parallel polarizers (oriented at 0° from the x axis). The white scale bar (top left of the first image) measures $10\,\mu\mathrm{m}$.

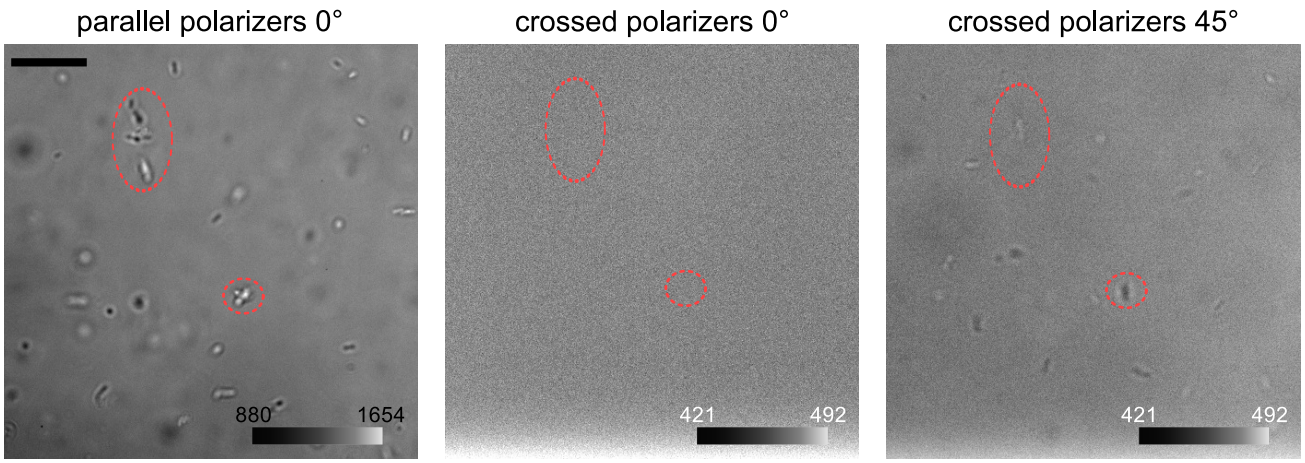

Figure S7: Sequence of images taken from a sample of bacteria with 8.2 wt% of DSCG showing two aggregates of bacteria (circled in red) in the medium (far from surfaces). The black scale bar (top left of the first image) measures 20 μm. Note the different intensity scale between the first image and the other two. This shows that the aggregates of bacteria are not caused by local inhomogeneities in the medium.

S5.2 Nematic phase

This section shows bright field images of microspheres in DSCG solutions (in MB) in the nematic phase and in the transition zone. The angle between the first polarizer and the axis of the director (the x axis in Fig. S8) is reported on top of each image, and the intensity scale is at the bottom right. From the images to the right of Fig. S9 we can conclude that DSCG aggregates in samples were well aligned (the intensity is high and uniform). All experiments were made at $22.5 \pm 0.5\,^{\circ}$C.

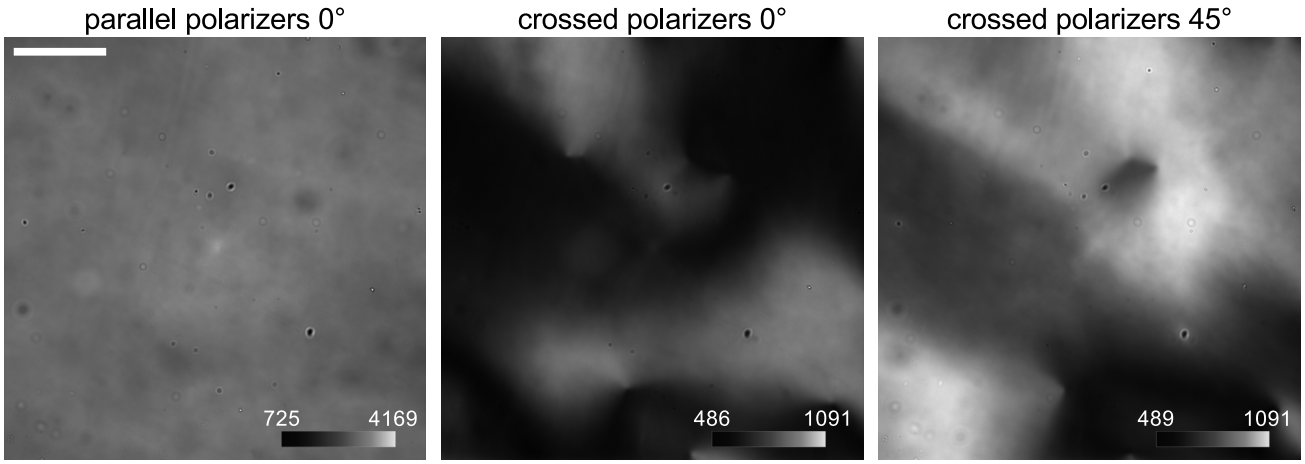

Figure S8: Images taken from a sample of microspheres with a diameter of $0.75\,\mu$m in a solution with 10.2 wt% of DSCG. The image presents a nematic section of the sample that was not well aligned, this is why the intensity is not uniform. The white scale bar (top left in the first image) measures $50\,\mu$m.

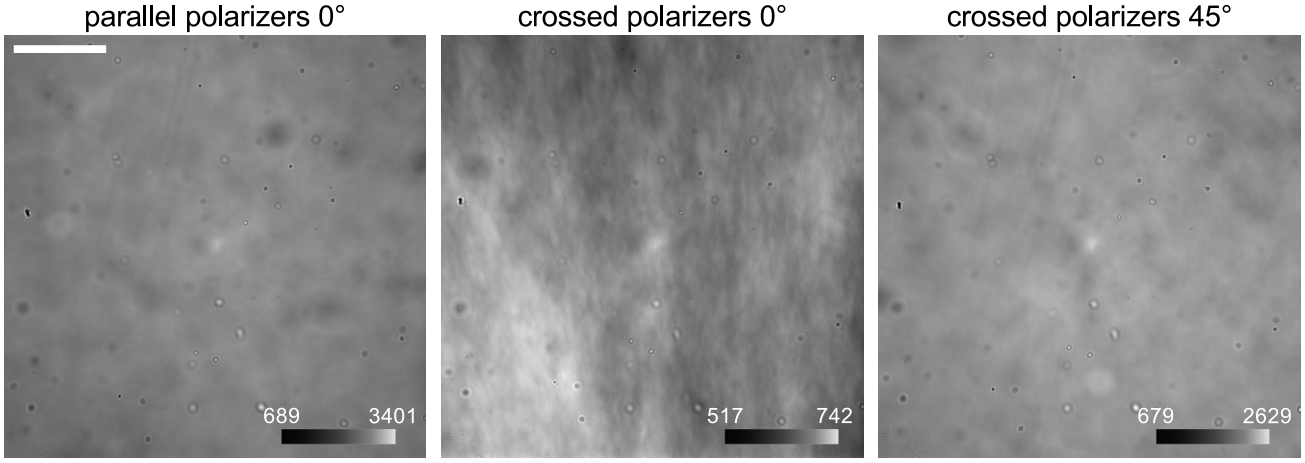

Figure S9: Images taken from a sample of microspheres with a diameter of $0.75\,\mu$m in a solution with 13.2 wt% of DSCG. The white scale bar (top left in the first image) measures $50\,\mu$m.

S6 Additional figures and tables

Table S3: Number of tracked bacteria and total number of recorded positions for each DSCG concentration.

Concentration (±0.2) (wt %)	Number of tracked bacteria	Total number of recorded positions
0	426	12265
1	221	6823
2.1	189	4973
3.2	134	3583
4.2	166	5981
5.3	180	6964
6.3	101	4112
7.4	85	3157
8.4	41	2519
9.5	37	2843
10.5	111	11616
11.6	40	6805
12.6	34	4393
13.7	43	7916

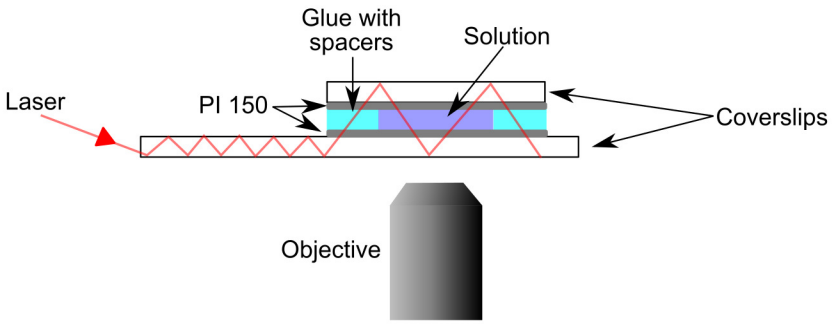

Figure S10: Scheme of a cell used for the observation of bacteria and for the measurement of DSCG solution's viscosity. The principle of light guided dark-field microscopy is illustrated with the laser beam (see also [3]).

Table S4: Constants used for the calculation of the DSCG aggregates length.

Constant name	Symbol	Value or equation
Viscosity at 0 wt%	η_0	$0.96\,\mathrm{g/m \cdot s}$
Viscosity of the solution	η	—
Relative viscosity	η_r	$\frac{\eta}{\eta_0}$
Radius of DSCG disk	r	1 nm
Thickness of DSCG disk	d	0.34 nm
Stokes radius of DSCG disk	r_p	0.55 nm
Volume fraction of molecule in aggregates	ϕ_m	0.9
Volume fraction of DSCG	ϕ	—
Fractal dimension of aggregates	d_f	1
Hydrodynamic volume of aggregates	v_h	$\frac{M}{N_a}$

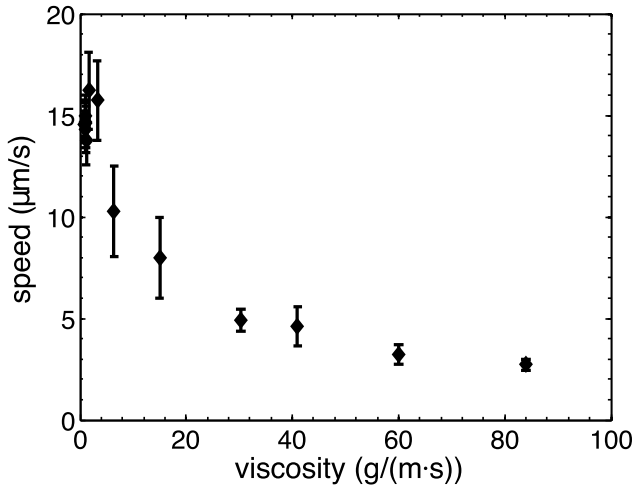

Figure S11: Speed of the bacteria as a function of the viscosity parallel to the director.

SUPPORTING REFERENCES

[1] Turiv, T., I. Lazo, A. Brodin, B. I. Lev, V. Reiffenrath, V. G. Nazarenko, and O. D. Lavrentovich. 2013. Effect of collective molecular reorientations on brownian motion of colloids in nematic liquid crystal. *Science*. 342:1351–1354.

[2] Berezhkovskii, A. M., L. Dagdug, and S. M. Bezrukov. 2014. Discriminating between anomalous diffusion and transient behavior in microheterogeneous environments. *Biophys. J.* 106:L09–L11.

[3] Duchesne, I., S. Rainville, and T. Galstian. 2015. Application of a microrheology technique to measure the viscosity of disodium cromoglycate liquid crystal. *Mol. Cryst. Liq. Cryst.* Submitted.

[4] Sowa, Y. and R. M. Berry. 2008. Bacterial Flagellar Motor. *Q. Rev. Biophys.* 41:103–132.

[5] Martinez, V. A., J. Schwarz-Linek, M. Reufer, L. G. Wilson, A. N. Morozov, and W. C. K. Poon. 2014. Flagellated bacterial motility in polymer solutions. *Proc. Natl. Acad. Sci. USA*. 111:17771–17776.

[6] Purcell E. M. 1997. The efficiency of propulsion by a rotating flagellum. *Proc. Natl. Acad. Sci. USA*. 94:11307–11311.

[7] Chattopadhyay, S., R. Moldovan, C. Yeung, and X. L. Wu. 2006. Swimming efficiency of bacterium *Escherichiacoli*. *Proc. Natl. Acad. Sci. USA*. 103:13712–13717.

[8] Mao, Y., M. E. Cates, and H. N. W. Lekkerkerker. 1997. Theory of the depletion force due to rodlike polymers. *J. Chem. Phys.* 106:3721–3729.

[9] Yaman K., C. Jeppesen, and C. M. Marques. 1998. Depletion forces between two spheres in a rod solution. *Europhys. Lett.* 42:221

[10] Hadjur, C., N. Lange, J. Rebstein, P. Monnier, H. van den Bergh, and G. Wagnières. 1998. Spectroscopic studies of photobleaching and photoproduct formation of *meta*(tetrahydroxyphenyl)chlorin (*m*-THPC) used in photodynamic therapy. The production of singlet oxygen by *m*-THPC. *J. Photochem. Photobiol. B, Biol.* 45:170–178

[11] Heiser, I., W. Oßwald, and E. F. Elstner. 1998. The formation of reactive oxygen species by fungal and bacterial phytotoxins. *Plant Physiol. Biochem.* 36:703–713

[12] Kumar, A., T. Galstian, S. K. Pattanayek, and S. Rainville. 2013. The motility of bacteria in an anisotropic liquid environment. *Mol. Cryst. Liq. Cryst.* 574:33–39.